Cleaning of complex soil layers on vertical walls by fixed and moving impinging liquid jets

Glover, H.W., Brass, T., Bhagat, R.K., Davidson, J.F., Pratt, L. and Wilson, D.I.

Department of Chemical Engineering and Biotechnology, New Museums Site, Pembroke Street, Cambridge, CB2 3RA, UK

Submitted to

Journal of Food Engineering

Revised Manuscript

December 2015

Corresponding author

D. Ian Wilson

Tel: +44 1223 334 791

E-mail: diw11@cam.ac.uk

Cleaning of complex soil layers on vertical walls by fixed and moving impinging liquid jets

Glover, H.W., Brass, T., Bhagat, R.K., Davidson, J.F., Pratt, L. and Wilson, D.I.

Department of Chemical Engineering and Biotechnology, New Museums Site, Pembroke Street, Cambridge, CB2 3RA, UK

Abstract

Cleaning by a horizontal water jet, impinging onto a soiled Perspex vertical plate, is described. The plate, the *substrate*, was coated with PVA or petroleum jelly, the *soil*. The substrate was either

(i) fixed, for batch tests in which the cleaned area, roughly circular, grew with time, or

(ii) the substrate moved vertically up or down in its own plane, the water jet remaining fixed; this reproduced the effect of a jet moving across a surface for cleaning, as found in real tank cleaning operations.

In the batch experiments, growth of the radius a of the cleaning area is well described, at early times t, by $a^5 - a_o^5 = K^5 (t - t_o)$, a_o being the initial radius of the cleaned area at time t_o; K is a constant. At later times with petroleum jelly, the cleaning front reached a maximum value, when the outward momentum of the radially flowing water film balanced the strength of the soil. This maximum value is modelled as a ramp of viscoplastic soil inclined at angle χ to the substrate surface, where χ was found to vary from 7° to 25°.

In the tests of continuous cleaning of petroleum jelly, a lengthening cleaned area, of width w_c, was observed on the moving substrate. Near the jet was a stationary clean front, whose shape looked like half an ellipse. This shape, and the width w_c, are well described by theory (Wilson *et al Chem. Eng. Sci.* 2015, **123,** 450–459) using parameters from the above-mentioned batch experiments. This establishes a good link between batch and continuous cleaning experiments.

Keywords Cleaning, fluid mechanics, impinging jet, PVA, petroleum jelly, viscoplastic

Introduction

Cleaning is an important step in any food manufacturing process, whether to clear away residual material from process equipment at product changeover or to remove fouling deposits which can affect process operability, product quality or hygienic operation (Fryer and Asteriadou, 2009). Automated plant makes increasing use of cleaning-in-place (CIP) operations, wherein material is removed by the action of recirculating rinse washes, cleaning solutions and disinfectants. Time spent cleaning represents a loss of production, affecting the financial sustainability of a plant. Cleaning affects the environmental sustainability in terms of energy consumption (cleaning solutions are frequently heated) and material (provision of cleaning chemicals and disposal of wastes, as well as neutralisation of acid and alkaline agents) (Köhler *et al*., 2015). There is thus a need to optimise the performance of cleaning operations.

Much of the research into CIP mechanisms to date has concentrated on enclosed units, *e.g*. pipes, heat exchangers, where the flow of cleaning solutions is well understood. The food industry makes extensive use of tanks and similar vessels for storage, mixing, reaction and heating, for which 'fill and soak' cleaning operations take long times and require large volumes of liquid. Some systems use moving[1] jets of liquid, created by nozzles or lances, to distribute cleaning solution across the walls of process vessels at higher velocities than in standard pipe flows so that cleaning is augmented by hydraulic action (Jenssen, 2011). These can significantly reduce the time to clean a vessel.

There has, however, been relatively little work to date on cleaning of surface layers – which we refer to here as soiling layers – by impinging liquid jets. Meng *et al*. (1998) and Leu *et al*. (1998) studied the mechanisms of removing surface coatings by high velocity waterjets (which formed sprays). Burfoot and co-workers (Burfoot and Middleton, 2009; Burfoot *et al*., 2009) quantified the effectiveness high pressure jets in food cleaning applications. Yeckel and Middleman (1987) studied and modelled the removal of viscous (oil) films from horizontal surfaces by a vertical impinging water jet in the region bounded by the hydraulic jump; in this region the liquid flows outwards in a thin film and subjects the layer to significant shear forces. Lately, Walker and co-workers (Hsu *et al*., 2011; Walker *et al*.,

[1] The terms 'moving' and 'fixed' in this paper refer to the relative motion of the nozzle. The liquid is in steady continuous flow.

2012) have extended this approach and considered the interaction of such jets on layers of non-Newtonian fluids.

The knowledge of cleaning mechanisms gained from the above studies is expected to apply to cases where the soiling material is attached uniformly to a wall, but the flow behaviour of the liquid changes noticeably as it moves over a vertical (or inclined) wall. When a liquid jet hits a flat surface, it spreads out radially as a thin, fast moving film (termed the *radial flow zone*, RFZ) until a point where the thickness of the jet increases abruptly. When the liquid impinges downwards on a horizontal plate, this change in thickness is called a *hydraulic jump* and the flow pattern is symmetric. When a jet strikes a vertical wall a similar feature is formed above the point of impingement, which we call the *film jump*. Beyond the film jump the liquid flows downwards, moving around the film jump as a *rope* which increases in thickness. These features are shown in Figure 1(*a*). Below the point of impingement the liquid flows downwards as a wide film, bounded by a rope on each side. The film can stay wide or narrow further downstream, depending on the wetting characteristics of the surface (Aouad *et al*., 2015). These flow patterns and quantitative models for predicting their dimensions and behaviour have been studied for jets impinging on stationary walls by Wilson and co-workers (Wilson *et al*., 2012; Wang *et al*. 2013a; 2013b; 2015).

Fouling layers and residues in the food sector are often complex soft solids (Fryer and Asteriadou, 2009). Knowledge of cleaning mechanisms has been driven by the need to understand and optimise CIP systems, particularly duct flows (*e.g.* Gillham *et al*., 1999; Fryer *et al*. 2006). The removal of soil layers by impinging jets can involve *adhesive* and/or *cohesive* mechanisms. In the former, the forces imposed by the liquid are sufficient to overcome the strength of attachment of the layer to the substrate and the layer is peeled off: it may fragment as part of this process, depending on its strength (*i.e*. the interactions between elements of the soil). With cohesive removal, the forces imposed by the liquid are sufficient to fragment the soil, *i.e*. by erosion or delamination. The soil is worn away until the substrate is reached. Dissolution, enhanced by convective mass transfer, may also occur. Wilson *et al*. (2014) studied the adhesive removal of soils by fixed impinging jets, where a circular, cleaned region grows outwards from the point of impingement. They presented a quantitative model, using results from the hydrodynamic model of Wilson *et al*. (2012), which gave a good description of data obtained for layers of polyvinyl acetate (PVA), Xanthan gum, and petroleum jelly. They subsequently extended this model (Wilson *et al*., 2015) to describe the cleaning action of a liquid jet moving across a soiled plate and were able to predict the shape of the cleaned front and the trends observed for Xanthan gum layers reported by Köhler *et al*. (2015).

This ability to predict the liquid contacting pattern and the shape of the cleaned front (see Wilson *et al*., 2015) is critical for detailed simulation of cleaning by impinging jets. Knowledge of the liquid contacting pattern allows the regions wetted by the cleaning solution to be identified, as well as the time that the layer is in contact with solution: soaking time and reaction with a cleaning agent are important factors in the removal of complex soils (Wilson, 2005; Fryer and Asteriadou, 2009). Knowledge of the shape of the cleaned front allows the area cleaned by a moving jet to be calculated for different trajectories, so that these can be optimised.

This paper presents an extension of the above experimental and modelling studies in two aspects. The first is the use of a new experimental configuration which allows the shape of the cleaned front and the flow patterns to be determined in real time. In previous studies (Köhler *et al*., 2015; Wilson *et al*., 2015) the jet had to be interrupted in order to determine the shape of the cleaned front. In the current work, the jet is stationary but the soiled plate is moved upwards (or downwards) past the jet while being videoed.

Moving surfaces and stationary nozzles have been employed by workers such as Gradek *et al*. (2006) to study hydraulic jump behaviour but have not, to the authors' knowledge, been used to study cleaning, particularly for vertical surfaces. The second aspect is the study of more complex soils, specifically layers of non-crosslinked PVA and a petroleum jelly. The influence of layer thickness is here investigated for both materials. The adhesive removal model of Wilson *et al*. is adapted to describe the removal of the petroleum jelly, which is a viscoplastic material (Ali *et al*., 2015).

Models

Radial flow zone hydrodynamics

In these experiments cleaning is observed within the radial flow zone, where the liquid flows as a thin fast moving film. Wilson *et al*. (2012) modelled the flow in the RFZ as a Nusselt film, with the average velocity, U, at radius r given by

$$\frac{1}{U}-\frac{1}{U_o}=\frac{10\pi^2\mu}{3\rho Q^2}\left[r^3-r_o^3\right] \qquad [1]$$

Here U_0 is the velocity in the impinging jet of radius r_0, Q is the jet volumetric flow rate, ρ is the liquid density and μ its dynamic viscosity. The momentum in the liquid film per unit circumferential width, M, at radius r is

$$M=\frac{3\rho Q}{5\pi}\frac{U}{r} \qquad [2]$$

They calculated the location of the film jump, R, from a force balance in which the outward flow of momentum was balanced by surface tension, γ, acting along the surface and at the liquid-substrate contact line (with contact angle β). Assuming that $U_0 \gg U(R)$ and $R \gg r_0$ gave

$$R=0.276\left[\frac{\rho^2 Q^3}{\mu\gamma(1-\cos\beta)}\right]^{1/4} \qquad [3]$$

This result is compared with the experimental data for jets impinging on moving substrates.

Cleaning – static jets

Wilson *et al*. (2014) presented a model to describe the adhesive (removal) of soil within the RFZ by a static jet. Material is removed to leave a circular clean region of radius a, as shown in Figure 1(*b*). The rate of growth of the cleaned region is postulated to be proportional to the force imposed by the fluid, which is a fraction of the momentum per unit width, M, at a:

$$\frac{da}{dt}=k'M \qquad [4]$$

where t is time and k' is a cleaning rate constant, expected to be related to the soil thickness, δ. The influence of initial soil layer thickness on cleaning rate is investigated for layers of PVA and petroleum jelly here.

The momentum flux per unit width, M,is estimated using Equations [1] and [2], assuming that $1/U_o$ is small, replacing r by a in Equation [1] and assuming $a \gg r_o$; this gives

$$\frac{da}{dt} = \frac{3k'\dot{m}^3}{\pi c}\frac{1}{5a^4} = K^5\frac{1}{5a^4} \qquad [5]$$

Here, $\dot{m}$ is the mass flow rate, c is a constant determined by liquid properties ($c = 10\pi^2\rho\mu/3$), and K a flow rate dependent cleaning rate constant. Integrating [5] from the point where a circular cleaning front is first observed, a_o, at time t_o gives with $\Delta t = t - t_o$,

$$a^5 - a_o^5 = K^5(t - t_o) = K^5\Delta t \qquad [6]$$

Wilson *et al.* (2014) showed that Equation [6] described the evolution of the cleaned front for several materials until the radius a reached the film jump, when Equations [1], [2] and [3] no longer apply. In the current work Equation [6] is fitted to data obtained with layers of different thickness to determine the effect of δ on K (and hence k', where tests are conducted using different flow rates).

Cleaning – moving jets

In this case the nozzle moves relative to the substrate at velocity v_{jet}. Wilson *et al.* (2015) adapted the above static jet cleaning model to allow for relative motion between the substrate and the jet, for the case where $|U_o| \gg |v_{jet}|$. The shape of the cleaned region is shown schematically in Figure 1(*c*). The jet impinges at point O: ahead of O there is an almost parabolic cleaning front centred on O, which extends into the jet wake and leaves a swathe of width w_c. By considering the locus of stationary points directly preceding the jet (the dashed line in Figure 1(*c*)) where the rate of peeling matches that of the approaching foulant, the following ODE describing the shape of the cleaning front is obtained:

$$\frac{dp}{d\theta} = \frac{1}{5}\frac{K^5}{v_{jet}}\frac{1}{p^3\sin\theta} - \frac{p}{\tan\theta} \qquad [7]$$

Here, p is the radial distance from O to the cleaning front and θ the azimuthal angle measured anticlockwise from the nozzle traverse direction. Integrating [7] from $\theta = 0$ to 180° gives the shape of the cleaning front: there is a maximum in the half-width at $\theta = 127°$, which enabled Wilson *et al.* to predict the width of the cleared region downstream of the moving jet, *viz.*

$$\begin{aligned} w_c &= 2.94\left(\frac{K^5}{5}\frac{1}{v_{jet}}\right)^{1/4} \\ &= 1.97\frac{K^{5/4}}{v_{jet}^{1/4}} \end{aligned} \qquad [8]$$

This result is tested for the moving plate configuration, for petroleum jelly layers.

Cleaning – viscoplastic soils

Equation [5] predicts that the size of the cleaned region should increase steadily until a reaches R, the limit of the RFZ. Hodgson and Smith (2014) studied the removal of layers of petroleum jelly in the apparatus used by Wilson *et al*. (2014) and observed that a often reached a limiting value, a_{max}, where $a_{max} < R$. They attributed this to the viscoplastic nature of the soil, wherein a yield stress must be overcome before the material will yield. They proposed a quantitative model of this behaviour and the following analysis builds on their model.

At the cleaning front the flow of liquid dislodging the material is assumed to cause yield along a flat shear plane inclined to the substrate surface at angle χ (see Figure 2). This front moves radially outwards with time when the force imposed by the liquid film is sufficient to overcome the yield strength. Beyond a the liquid flows upwards so that a fraction of its momentum flux is no longer horizontal and the difference between M and $M\cos\chi$ provides the driving force for cleaning (see Equation [4]). When the cleaning front reaches a_{max}, the net momentum flux is equal to the force required to overcome the shear yield stress of the layer and induce motion. The area of the yielding region for a complete circle of radius a_{max}, *i.e*. the ramp face, is approximately $2\pi a_{max}\delta/\sin\chi$: the length of the ramp is assumed to be small compared to a_{max}. A force balance in the horizontal direction at a_{max} gives

$$\frac{6}{5}\left(\dot{m}U - \dot{m}U\cos\chi\right) = \tau_y\left(\frac{2\pi a_{max}\delta}{\sin\chi}\right)\cos\chi \qquad [9]$$

where τ_y is the shear yield stress of the layer; the coefficient 6/5 arises from considering the momentum flux due to the parabolic velocity profile in the liquid film, as in Equation [2] (see Wilson *et al.*, 2012). Substituting for U from Equation [1], with $1/U_o$ and r_o both small and $r = a_{max}$, yields

$$a_{max} = \left(\frac{3\dot{m}^3}{5\pi c} \frac{1}{\tau_y \delta} \left[\tan\chi - \sin\chi \right] \right)^{1/4} . \qquad [10]$$

An alternative form of Equation [4] is now proposed to describe the rate of cleaning of a yield stress material:

$$\frac{da}{dt} = k'(M - M_Y) \qquad M > M_Y \qquad [11a]$$

$$\frac{da}{dt} = 0 \qquad M \le M_Y \qquad [11b]$$

where M_Y is the momentum flux required to cause yield.

By constructing a momentum balance per unit circumferential width in the radial direction, the change in fluid momentum can be equated to the force required to yield the material at radius a. With a flat shear plane of area per unit width $\delta \operatorname{cosec}\chi$ inclined an angle χ, this gives an expression for M_Y, *viz*.

$$M_Y - M_Y \cos\chi = \tau_y (\delta \operatorname{cosec}\chi) \cos\chi \qquad [12]$$

which yields

$$M_Y = \frac{\tau_y \delta}{(\tan\chi - \sin\chi)} \qquad [13]$$

To integrate Equation [11a], M is obtained from Equation [5], derived from Equation [4]; M_Y is obtained by substituting $\tau_y\delta$ from Equation [10] into Equation [13], giving $M_Y = 3\dot{m}^3 / 5\pi c a_{max}^4$. Combining this with Equations [11a] and [5] gives

$$\begin{aligned} \frac{da}{dt} &= k' \frac{3\dot{m}^3}{5\pi c} \frac{1}{a^4} \left(1 - \left(\frac{a}{a_{max}} \right)^4 \right) \\ &= \frac{K^5}{5a^4} \left(1 - \left(\frac{a}{a_{max}} \right)^4 \right) \end{aligned} \qquad a < a_{max} \qquad [14]$$

in which K is a lumped cleaning rate constant. The growth of the cleaned region is given by

$$t - t_o = \frac{5}{K^5} \int_{a_o}^{a} \frac{a^4}{1 - (a/a_{\max})^4} da \qquad [15]$$

For the case where $a = 0$ when $t = 0$, Equation [15] yields

$$t = \frac{5}{4}\left(\frac{a_{\max}}{K}\right)^5 \left\{ \ln\left(\frac{1 + a/a_{\max}}{1 - a/a_{\max}}\right) - 4\left(\frac{a}{a_{\max}}\right) + 2\tan^{-1}\left(\frac{a}{a_{\max}}\right) \right\} \qquad [16]$$

For other cases, as observed here, employing a Taylor expansion in $a/a_{\max}$ and integrating the above integral gives

$$t - t_o = \left(\frac{a_{\max}}{K}\right)^5 \left\{ \left(\frac{a}{a_{\max}}\right)^5 - \left(\frac{a_o}{a_{\max}}\right)^5 + \frac{1}{9}\left(\frac{a}{a_{\max}}\right)^9 - \frac{1}{9}\left(\frac{a_o}{a_{\max}}\right)^9 + \frac{1}{13}\left(\frac{a}{a_{\max}}\right)^{13} - \frac{1}{13}\left(\frac{a_o}{a_{\max}}\right)^{13} + \ldots \right\} \qquad [17]$$

The terms containing ($a_o/a_{\max}$) are usually negligible. In the early stages of cleaning, Equation [17] reduces to Equation [6], which was fitted to the data in this linear region to give K. With this value of K, $a_{\max}$ was then obtained by fitting Equation [17] to data points (see Figure 12) over the whole range of $\Delta t^{0.2}$. Each value of $a_{\max}$ then gave χ from Equation [10], using $\tau_y = 50$ Pa and the measured soil thickness δ.

Both equations [15] and [17] reduce to Equation [6] when $a/a_{\max}$ is small. This was the case for the experiments on removing petroleum jelly with moving jets in this work, so Equation [8] is used to analyse those data.

Materials and Methods

Impinging jet apparatus

The apparatus was based on that reported by Wang *et al.* (2013b), see Figure 3. The nozzle and target were mounted inside a 1.2×1.2×1.7 m high cabinet with Perspex sides which allowed the jet and substrates being cleaned to be videoed through the walls. Reverse osmosis (RO) water at room temperature (approximately 20°C) was pumped from a 26 litre holding tank though a rotameter, control valve and flexible tubing before entering a 150 mm straight entry section upstream of the nozzle. Brass nozzles with bore diameter, d_N, of 2, 3 and 4 mm were available: a 2 mm nozzle was used in the cleaning tests reported here. The nozzle was positioned 60 mm from the target in order to ensure that the jet was coherent. The alignment of the nozzle and target was checked regularly using a square and a digital inclinometer.

An interrupter plate was located between the nozzle and the target in the initial period while flow was set and stabilised. The plate was then removed to start a cleaning test. After striking the target, the water drained vertically, fell to the cabinet floor and was either discharged to drain or recycled if no soil was entrained.

Video recordings of jet impingement and cleaning were made using a Nikon D3300 D-SLR digital camera aligned normal to the target. Images were processed using the NIH ImageJ software. Transparent graticule tape was located on the reverse (dry) side of target sheets in order to provide length calibration. Illumination was provided by external 1200 W halogen lamps or a waterproof IP65 (240V, 36 W) tube light.

Targets for static jet cleaning were held in an aluminium frame which could be positioned at different distances from the nozzle. Sheets (glass or Perspex) of dimensions 360×600×5 mm (width×height×depth) were coated separately and mounted on the frame using locating screws.

Cleaning by moving jets was studied using the arrangement shown in Figure 3 in which the nozzle remained stationary and the target was moved upwards or downwards in order to generate relative motion between the two. This configuration allowed the flow pattern and cleaning region to be videoed by a stationary camera, and nozzle-motion-induced vibration in the jet eliminated. A ‘sash window’ system, using a rubber-toothed drive belt connected to a two-way variable speed motor, provided the vertical motion of the target plate. Cut-off switches were located on the belt drive to avoid the target exceeding its maximum travel on the frame. Calibration tests determined that the target plate reached its steady velocity after an initial 100 mm of travel so cleaning experiments were not started until this acceleration stage had been completed. This allowed 500 mm of traverse at constant speed, at speeds up to 250 mm s^{-1}.

Target plate preparation

Soil layers were prepared from two materials on glass or Perspex plates. The uniformity (flatness and thickness) of the plates was checked using a Moore & Wright deep throat digital micrometer at 24 different locations on the plate. Two materials were considered for preparing soil layers, namely a water-based PVA glue (ASDA supermarket brand) and petroleum jelly (Trilanco White Petroleum Jelly, Poulton-le-Flyde, UK). The former interacts with the cleaning agent (water), undergoing swelling, while the latter is hydrophobic and does not interact. The PVA tended to pool towards the plate edges when spread over glass so only Perspex substrates were used in the PVA tests.

The rheology of the petroleum jelly was investigated with a Bohlin CV-120 controlled stress rheometer using sand-blasted 50 mm diameter parallel plates with a 1 mm gap. The petroleum jelly did not exhibit simple viscoplastic behaviour: steady shear tests indicated a high viscosity, low-shear plateau marked by a transition to shear thinning at approximately 50 Pa. Oscillatory stress tests were performed at a frequency of 1 Hz and these showed a transition from elastic to viscous behaviour around 50 Pa. This value was used as the yield stress for the petroleum jelly in the model calculations. By comparison, the petroleum jelly product used by Wang (2014) had a yield stress of 12 Pa (see Yang *et al*., 2012).

Even soil layers were prepared by dragging a 340 mm aluminium slider blade over the surface, leaving a uniform layer of soil in its wake. The clearance between the blade and the plate was adjusted by a pair of micrometers located behind the drag wheels (see Figure 4), to give film thickness from 50-2000 μm.

PVA layers were applied and left to dry in air at ambient temperature for 24 h. Measurements of the mass of 120 μm thick layers over time indicated an exponential decrease in mass over the first 3.5 h, to approximately 21% of the original value. The thickness of the dry PVA layer was checked using the digital micrometer at 24 locations.

Petroleum jelly layers were prepared on Perspex or borosilicate glass plates. The micrometer could not be used to determine the thickness of the petroleum jelly layers as the material is soft, so the thickness of the layers was estimated by measuring the mass of jelly applied and determining its thickness from the area covered and the density, measured separately as 870 ±5 kg m^{-3}. This calculation relies on the substrate being perfectly flat, so a conservative estimate of its precision, of 50 μm, is quoted. The yield stress of the jelly was measured previously as 12 Pa at 20°C (Yang *et al*, 2013).

The PVA layers were colourless when dry but turned white and swelled when contacted with water. The influence of PVA layer thickness on swelling and deformation behaviour was studied using fluid dynamic gauging (FDG, see Wang and Wilson, 2015), which allows the swelling of a coating immersed in liquid to be monitored in situ and in real time. The layer thickness is measured by recording the pressure drop in a liquid being sucked through a nozzle at a given flow rate, the nozzle being located close to the layer surface. FDG measurements were performed using the automated apparatus described by Wang and Wilson (2015) with a 1 mm nozzle diameter and RO water at 20°C as the gauging fluid. PVA layers of various thicknesses were prepared on stainless steel discs and dried as described above. The loss of mass on drying, and the thickness of the dried layer, were recorded. These indicated similar behaviour to the layers prepared on Perspex surfaces. Measurements were recorded for up to an hour following immersion of the sample in the test chamber. It took up to 60 s to fix the plate and establish the gauging flow, so the initial stage of swelling could not be monitored.

Results and Discussion

Film jump location

The location of the film jump and the extent of the rope region, *i.e.* the distances R and R_c at the level of jet impingement (A-A in Figure 1(a)), were measured for coherent jets generated by all three nozzles (d_N = 2, 3, 4 mm) and different flow rates. The experimental measurements of R were in reasonable agreement with the predictions of Equation [3] using an effective contact angle of 90°, as reported in previous studies (Wang *et al*. 2013b; Wilson *et al*., 2014). These results are presented in Supplementary Figure S1 and provide confidence in using Equation [2] to estimate the local momentum flux.

The effect of substrate motion on the size of the film jump was studied for the configuration employed in the moving jet cleaning studies (water impinging on Perspex at 20°C, d_N = 2 mm, Q = 35 mL s^{-1}; Re_{jet} = 21,700) with nozzle liquid velocities up to ±233 mm s^{-1}. For a static jet (v_{jet} = 0), R was 46 mm, as shown by the broken line in Figure 5; the diagram also shows that R increased a little with v_{jet} when the plate was moving upwards, *i.e.* the jet impinged on a region already wetted. Conversely, R decreased a little when the plate was moving downwards. With reference to Equation [3], this indicates that the effective contact angle is affected by the motion of the contact line. A second factor is the relative velocity between the incoming jet and the target plate, which gives rise to different, non-orthogonal, angles of impingement for the upward and downwards moving jets. For the present work, the jet trajectory is always perpendicular to the the plate, whatever the relative values of jet velocity, U_o, and nozzle travel speed, v_{jet}. Here, $U_o \gg v_{jet}$, so the film velocity in the RFZ was assumed to be the same as for a stationary jet (when $v_{jet} = 0$). If was comparable with U_o, a new RFZ analysis would be needed. Wang *et al.* (2014) studied the effect of angle of impingement on R: values below 90° (jet pointing slightly downwards) gave smaller R owing to a larger fraction of the flow moving downwards, away from the point of impingement. The effective angles of impingement, calculated for a plate velocity of 52 mm s^{-1}, nozzle diameter 2 mm and flow rate 35 mL s^{-1}, were 89° and 91° for downward and upward moving plates, respectively. With a plate velocity of 233 mm s^{-1} the effective angle of impingement was calculated as 85.2° and 94.8° for downward and upward moving plates, respectively. These angles are near enough to 90° to justify the assumption of perpendicular impingement.

The observed reduction in RFZ width with increasing downward plate velocity is qualitatively consistent with the results presented by Gradeck *et al.* (2006) using a fixed nozzle and a fast moving belt as the substrate. They employed nozzle velocities (relative to the belt) of similar magnitude to the average velocity of liquid in the jet, and quantified the effect of the nozzle motion on the curvature of the hydraulic jump rather than the location of the jump.

The rope was noticeably more stable for a downward moving jet, *i.e.* an upwards moving plate. In this case the flow is passing over a surface which had been previously wetted by liquid and conditions at the contact line are expected to be related to phenomena affecting the receding contact angle, such as better wetting (smaller contact angle).

Cleaning PVA films – static nozzle

Vertical Perspex sheets, each coated with a PVA layer of dry thickness 16-171 μm were cleaned by a horizontal water jet (Re_{jet} = 21,700, as above). For all layers, there was an initial contact time, t_c, before the jet broke through the soil and cleaning occurred by a peeling mechanism, sometimes involving ‘fingers’, see Figure 8. The formation of fingers in the RFZ has been reported previously, by Hsu *et al.* (2011), for water jets impinging perpendicularly on a layer of viscous liquid coating a solid plate. They observed longer and narrower fingering for elastic coating fluids (such as semi-dilute polyacrylamide solutions). Their findings are consistent with the present work as the PVA layer will have some elasticity: quantifying the elasticity of a swelling layer is a challenging topic.

Figure 6 shows that the contact time varied randomly with dry layer thickness for δ_{dry} values less than 75 μm. Above 75 μm there was an approximately linear relationship between δ_{dry} and t_c. Diffusion of water through the swelling PVA layer to the substrate/layer interface is thought to delay the onset of peeling; differences in the structure of the layer are also likely to affect the transition to peeling.

The FDG measurements presented in Figure 7 show a similar change in layer swelling behaviour with dry layer thickness. The data are reported as the swelling ratio, *S*, defined as $S = \delta(t)/\delta_{dry}$, where δ is measured by FDG and δ_{dry} by micrometer. Each data set shows a similar pattern, namely an initially rapid increase in thickness followed by a slow approach to an asymptotic level. Before the asymptote is reached, the thickness increases abruptly, marking a rupture event due to the stresses imposed by the gauging flow (in these tests, the maximum shear stress lay in the range 6-20 Pa, see Wang and Wilson (2015)).

There are noticeable differences in the amount of swelling (Figure 7) and the time taken for rupture (Figure 6) as δ_{dry} increases. The maximum swelling ratio is larger (and varies noticeably) with thinner layers, and rupture occurs earlier. The trend in rupture times reflects the observed trend in contact times in the cleaning experiments, and the former are plotted on a secondary axis alongside the t_c values in Figure 6. The FDG data complement the cleaning results.

The strength of the layer is expected to decrease as the layer swells (reducing the volume fraction of polymer), and rupture is expected to occur when the force imposed by the gauging flow exceeds the ability of the layer to resist it. The relationship between swelling ratio and layer strength is not yet known. A further factor is that cleaning is related to the strength of adhesion between the layer and the substrate: direct measurement of adhesion strength under cleaning conditions is difficult.

The initial stages of removal rarely featured a uniformly circular region, as assumed by the model (Equation [4]). Examples of the patterns observed are shown in Figure 8. The time at which a circular region, radius a_0, was formed is denoted t_0 (with $t_0 > t_c$) and the subsequent evolution of the size of the cleaned region was compared with the model. Supplementary Video 1 shows an example of cleaning of a PVA layer, starting from shortly before the film begins to be removed. There was generally good agreement with the form of the model, as shown by Figure 9 for two different layer thicknesses. In all cases the experiments were stopped before the size of the cleaned region, a, reached the film jump at R, when Equation [4] would not apply. The gradient of these loci yields the cleaning rate constant, K (Equation [5]). Figure 10 indicates that K was independent of δ_{dry}, which is expected for a cleaning mechanism involving peeling at the substrate-layer interface. The initial detachment behaviour, specifically whether fingering (see Figure 8(*a*,*b*)) was observed or not, is indicated by the symbol shading in Figure 10; there is no systematic influence on K. Further analysis indicated that K was independent of t_c (data not reported).

The values of K obtained in these tests (average 9.8 ± 2.0 mm $s^{-0.2}$: δ_{dry} = 20-170 μm) are similar to that of 12 mm $s^{-0.2}$ reported by Wilson *et al*. (2014) for PVA layers with dry thickness 120 μm. Their PVA glue was a branded product for consumer use, as in these tests. Detailed composition information was not available. Relating K (and k') to the properties of the layer and the substrate is the subject of ongoing work.

This work confirms that the modelling approach reported by Wilson *et al.* (2014) can be applied to materials with time-dependent response to cleaning solutions. In this case, the PVA layer had to undergo soaking for a given period – related to its thickness – before removal was observed. The dynamics of the PVA response to cleaning solution reflect behaviour such as pH-induced swelling and breakdown observed in many food systems. This time dependency will be important in CIP operations if regions higher up a wall are not wetted as much as regions below, over which falling films of cleaning solution are likely to flow continuously. The interaction between soaking and cleaning kinetics and jet hydraulics could be studied using the moving plate apparatus (Figure 3) but was not conducted for the PVA films in this study.

Cleaning petroleum jelly layers – static nozzle

Wilson *et al*. (2014) studied the removal of petroleum jelly layers using a range of nozzle sizes and flow rates. One nozzle size and flow rate were primarily used in the present work (Q = 35 mL s^{-1}, d_N = 2 mm, as in the PVA studies) in order to determine the influence of layer thickness and to test the modified cleaning model (Equation [15]).

Unlike the PVA layers, cleaning started as soon as the petroleum jelly was contacted by the impinging jet, giving a circular cleaned region (see Figure 11(*a*) and Supplementary Video

2). Dislodged jelly built up as a rim of spoil around the cleared region and gave rise to noticeable splattering and wayward jetting as this berm of material became thicker. The presence of the rim material did not affect the cleaning rate: this was confirmed by comparing tests at constant flow rate with ones where the flow was stopped momentarily after 20 s, the rim of material removed, and the flow restarted. The same maximum value, a_{max}, was reached in each case. This value was always smaller than the size of the RFZ expected for these flow conditions, of 46 mm.

The evolution of the cleaned region radius is plotted for two notionally identical tests in Figure 12, alongside data collected by Wang (2014) for a layer of a different petroleum jelly (on glass), albeit with initial thickness of 200 μm. The difference in behaviour for the notionally identical tests on glass illustrate the variability in the layers arising from the application method.

The data are plotted in the form suggested by Equation [6], with a_0 and t_0 set to zero (cleaning starts instantaneously), *i.e.* $a \propto t^{1/5}$. All three data sets follow a linear trend initially but then approach a limiting value asymptotically. Asymptotic behaviour is observed on Perspex and, (with a different asymptote) on glass, which is consistent with this asymptote arising from the viscoplastic nature of the soil. Each data set was fitted to Equation [15], adjusting χ (and hence a_{max}) to minimise the sum of squares of the error. The agreement with the fitted model is good, and the transition to asymptotic behaviour is captured reasonably.

Fitting the data to Equation [15] gives estimates of the lumped cleaning rate constant, K, and the final radius a_{max}. The former can also be obtained from the initial linear trend, as shown in Figure 12. The relationship between K and the soil layer thickness, δ, is presented in Figure 13(*a*), which shows a decrease in K with increasing soil thickness, particularly for thinner layers. The average value of K was 7.2 ±1.7 mm $s^{0.2}$, which is in reasonable agreement for the value of 6.1 mm $s^{0.2}$ reported by Wilson *et al.* (2014) for 250 μm petroleum jelly layers on Perspex cleaned with water at 20°C. The latter study did not explore the asymptotic behaviour observed with petroleum jelly. The K value of 7.2 ±1.7 mm $s^{0.2}$ corresponds to a k' value of 1.5×10^{-5} $kg^2m^{-4}s^{-1}$ (Equation [5]).

The Wang (2014) data, for a different petroleum jelly on borosilicate glass, yielded a K value of 13.3 mm $s^{0.2}$, which is significantly different from the values obtained with Perspex and confirms that the substrate-soil interaction is an important factor in determining the removal rate. The difference follows the trend expected from contact angle measurements: the petroleum jelly is strongly hydrophobic (contact angle > 90°) while the glass is more hydrophilic than Perspex (water contact angles of 33 ± 5° and 74 ± 5°, respectively).

The effect of layer thickness on cleaning rate is captured indirectly by the shear angle χ. The angle χ was calculated from Equation [10] assuming that $\tau_y = 50$ Pa. The data in Figure 13(*b*) show a linear relationship between χ and K. The values of χ are relatively modest, at less than 30°, indicating a gentle ramp at the point of peeling. It is noticeable that the χ value obtained from the Wang (2014) data set, with a different petroleum jelly on glass, differs from these on Perspex. It was not possible in these experiments to obtain accurate measurements of the shape of the cleaning front to confirm the assumption of a steady ramp profile. Both these results (and the correlation between K and χ evident in Figure 13(*b*)) indicate that the model requires further work, supported by measurements of the cleaning front employing small, detachable targets. Relaxing the assumption of simple viscoplastic behaviour for the soil would require detailed simulation of the coupled flow problem between a mobile soil and the cleaning liquid film.

Cleaning petroleum jelly layers – moving substrate, fixed nozzle

Experiments were performed with petroleum jelly layers of average thicknesses ranging from 295 to 1860 μm on vertical Perspex substrates. The jetting flow was the same as in the previous sections (water at 20°C, Q = 35 mL s^{-1}, d_N = 2 mm), with the vertical plate and substrate moving upwards or downwards, relative to the fixed horizontal cleaning jet, at velocities ranging from 6 to 31 mm s^{-1}.

As the jet passed over the soil, cleaning occurred immediately within the RFZ (see Figure 11(*b*) and Supplementary Video 3). The cleaning front was elliptical, as reported by Wilson *et al*. (2015), creating a cleared region of width w_c (see Figure 11(*b*)). This photograph also shows that a film jump was not observed in these tests as the berm of spoil deflected the water film away from the surface, giving splashback and secondary jetting. The cleaning front appeared to be more stable when the plate was moving downwards rather than upwards, which was accredited to the jet flowing into undisturbed soil. When the plate moved upwards, the soil had been in contact with the draining film prior to being washed by the jet.

The model of Wilson *et al*. (2015) (Equation [7]) was found to predict the shape of the cleaning front very well. Figure 14 compares the shape of the front extracted from photographs for several cases with the profile obtained by integrating Equation [7]. The results are presented in dimensionless form, scaled by a_x, the shortest distance from the impingement point to the cleaning front (see Figure 1(*c*)). The agreement with the predicted profile for upward moving jets is excellent, while there is more scatter with the downward moving jets, as mentioned above. The width of the cleaned region, w_c, was also less uniform when the jet was moving downwards, which could be due to the boundary of the RFZ buffeting the sides of the cleaned region as the nozzle descended.

Equation [8] indicates that w_c should be proportional to $v_{jet}^{-1/4}$. The data collected for two layer thicknesses are plotted in this form in Figure 15 and confirm this behaviour (as did data for other soil thicknesses, data not reported). These results confirm the generality of the Wilson *et al.* (2015) model, as it was developed to describe adhesive removal (peeling) of Xanthan gum layers.

Equation [8] is based on Equation [5], *i.e.* it does not consider the asymptotic behaviour resulting from the viscoplastic nature of the layer. Inspection of Figure 12 suggests that Equation [5] gives a reasonable description of petroleum layer behaviour when the radius of the cleaning front, which can be related to w_c /2, is less than $3a_{max}/4$. The values of w_c in Figure 15 (and the other data sets) all fitted this criterion so Equation [8] is expected to apply here.

Each datum in Figure 15 yields a value of K and these are compared with the values obtained for the static nozzle tests in Figure 16. There is excellent agreement between the two sets of results: both exhibit the decreasing trend with layer thickness discussed in the previous section. No further analysis of the shear plane shape is offered here. This result confirms that measurements made with the static nozzle can be used to predict the performance of moving jets, for both upwards and downwards cases.

velocities employed in these studies are low compared with those employed in industrial practice.

Conclusions

For batch cleaning by a horizontal water jet impinging on a vertical soiled surface, the growth of the radius a of the clean area for both soils considered here is well described, in the early stage of cleaning, by $a^5 - a_o^5 = K^5 (t - t_o)$; thus $(a^5 - a_o^5)^{0.2}$ is linearly related to $\Delta t^{0.2} = (t - t_o)^{0.2}$. The time t_o is when a clean area, of radius a_o, is first formed by the impinging jet. With the PVA soils, this time is related to swelling (and softening) of the layer, as demonstrated by separate fluid dynamic gauging tests. The initial removal of PVA layers was often, but not always, accompanied by fingering.

The value of the cleaning rate constant, K, was independent of dry layer thickness for the PVA soils, which is consistent with a peeling mechanism.

In contrast, K decreased with layer thickness for the petroleum jelly. With this soil, the radius, a, of the clean area approaches an asymptote a_{max}, when the radial momentum of the cleaning water film, formed by the jet impinging on the substrate, balances the adhesive strength of the soil on the substrate. The soil is modelled as forming a ramp at radius a_{max} which deflects the radial flow of cleaning water at angle χ to the substrate. The angle χ is calculated from a_{max} together with the soil thickness δ and its shear strength τ_y, measured separately. The angle χ is found to be of order 7 – 25 degrees; χ is linearly related to K.

Continuous cleaning was studied by moving the vertical soiled surface up or down relative to the horizontal cleaning jet, which was fixed. This simulated industrial cleaning where a jet moves over a soiled surface. The jet velocities and the nozzle velocities studied in these experiments are low compared to those employed in industrial practice: scale-up to industrial operating conditions represents an area for future work.

With the moving soiled plate, a cleaned strip, of width w_c, is formed; the clean strip is below the jet when the plate moves down, above the jet when the plate moves up. A cleaned front, of nearly semi-elliptical shape, is formed near the jet; the clean bit starts at distance a_x from the jet, above the jet with the plate moving down, below the jet when the plate moves up.

The width w_c, the distance a_x and the shape of the above-mentioned front are well predicted by the differential equation [7], using the parameter K from the batch experiments and the velocity v_{jet} of the substrate. In this way, the batch and continuous experiments are well linked; results from a batch experiment can be used to predict the behaviour of a continuous experiment where the cleaning jet moves parallel to the soiled plate.

Acknowledgements

Funding for RKB from the Commonwealth Scholarship Commission is gratefully acknowledged, as are helpful conversations with Michael Smith and Paul Hodgson. FDG measurements on the PVA layers were performed by Shiyao Wang.

References

Ali, A., de'Ath, D., Gibson, D., Parkin, J., Ward, G., Alam, Z. and Wilson, D.I. (2015) Development of a millimanipulation device to quantify the strength of food fouling deposits, *Food Bioproducts Proc*., **93**, 265-258

Aouad, W., Landel, J.R., Davidson, J.F., Dalziel, S. and Wilson, D.I. (2015) Particle image velocimetry and modelling of horizontal coherent liquid jets impinging on and draining down a vertical wall, submitted to *Experimental Thermal and Fluid Science*

Burfoot, D. and Middelton, K. (2009) Effects of operating conditions of high pressure washing on the removal of biofilms from stainless steel surfaces, *J. Food Eng*., **90**, 350-357.

Burfoot, D., Middelton, K. and Holah, J.T. (2009) Removal of biofilms and stubborn soil by pressure washing, *Trends Food Sci. Tech*., **20**, S45-S47.

Fryer, P.J, Christian, G.K., and Liu, W. (2006) How hygiene happens; the physics and chemistry of cleaning, Intl. J. Dairy Technology, **59**, 76-84.

Fryer, P.J., Asteriadou, K. (2009) A prototype cleaning map: a classification of industrial cleaning processes. *Trends in Food Science & Technology*, **20**, 225–262.

Gillham, C.R., Fryer, P.J., Hasting, A.P.M. and Wilson, D.I. (1999) Cleaning-in-place of whey protein fouling deposits: Mechanisms controlling cleaning, *Food Bioprod. Proc*., **77**, 127-136.

Gradek, M., Kouachi, A., Dani, A., Arnoult, D. and Borean, J.L. (2006) Experimental and numerical study of the hydraulic jump of an impinging jet on a moving surface, *Exptl. Thermal Fluid Sci*, **30**, 193-201.

Hsu, T.T., Walker, T.W., Frank, C.W. and G. G. Fuller, G.G. (2011) Role of fluid elasticity on the dynamics of rinsing flow by an impinging jet, *Phys. Fluids*. **23**, 033101.

Hodgson, P.J. and Smith, M.J. (2014) MEng Research Project Reports Department of Chemical Engineering and Biotechnology, University of Cambridge.

Jensen, B.B.B. (2011), Tank cleaning technology: Innovative application to improve clean-in-place (CIP), EHEDG Yearbook 2011/2012, 26-30.

Köhler, H., Stoye, H., Mauermann, M., Weyrauch, T., Majschak, J-P. (2015) How to assess cleaning? Evaluating the performance of moving impinging jets, *Food & Bioproducts Processing*, **93**, 327-332.

Landel, J.R., McEvoy, H. and Dalziel, S.B. (2015) Cleaning of viscous drops on a flat inclined surface using gravity-driven film flows, *Food Bioproducts Processing*, **93**, 310-317.

Leu, M.C., Meng, P., Geskin, E.S., Li, F. Tismenenskiy, L. (1998) Mathematical modelling and experimental verification of stationary waterjet cleaning process, *J. Manuf. Sci. Eng*., **120**, 571-579.

Meng, P., Geskin, E.S., Leu, M.C., Li, F. and Tismenenskiy, L. (1998) An analytical and experimental study of cleaning with moving waterjets, *J. Manuf. Sci. Eng*., **120**, 580-589.

Walker, T.W., Hsu, T.T., Frank, C.W. and Fuller, G.G. (2012) Role of shear-thinning on the dynamics of rinsing flow by an impinging jet, *Phys. Fluids*, **24**, 093102.

Wang, S. and Wilson, D.I. (2015) Zero discharge fluid dynamic gauging for studying the swelling of soft solid layers, *Ind. Eng. Chem. Res*., in press.

Wang, T., Davidson, J.F. and Wilson, D.I. (2013a) Effect of surfactant on flow patterns and draining films created by a horizontal liquid jet impinging on a vertical surface, *Chem. Eng. Sci*., **88**, 79-94.

Wang, T., Faria, D., Stevens, L.J., Tan, J.S.C., Davidson, J.F. and Wilson, D.I. (2013b) Flow patterns and draining films created by horizontal and inclined water jets impinging on vertical walls, *Chem. Eng. Sci*., **102**, 585-601.

Wang, T. (2014) Flow and cleaning behaviour of coherent liquid jets impinging on vertical walls, PhD Dissertation, University of Cambridge

Wang, T., Davidson, J.F. and Wilson, D.I. (2015) Flow patterns and cleaning behaviour of horizontal liquid jets impinging on angled walls, *Food Bioproducts Proc*., **93**, 333-342.

Wilson, D.I. (2005) Challenges in cleaning: Recent developments and future prospects, *Heat Transfer Engineering*, **26**(1), 51-59.

Wilson, D.I., Le, B.L., Dao, H.D.A., Lai, K.Y., Morison, K.R. and Davidson, J.F. (2012) Surface flow and drainage films created by horizontal impinging liquid jets, *Chem. Eng. Sci*., **68**, 449–460.

Wilson, D.I., Atkinson, P., Köhler, H., Mauermann, M., Stoye, H., Suddaby, K., Wang, T., Davidson, J.F. and Majschak, J-P. (2014) Cleaning of soft-solid soil layers on vertical and horizontal surfaces by coherent impinging liquid jets, *Chem. Eng. Sci*., **109**, 183–196.

Wilson, D.I., Köhler, H., Cai, L., Majschak, J-P. and Davidson, J.F. (2015) Cleaning of a model food soil from horizontal plates by a moving vertical water jet, *Chem. Eng. Sci.* **123**, 450-459.

Yang, Q., Ali, A, Shi, L. and Wilson, D.I. (2013) Zero discharge flow fluid dynamic gauging for studying the thickness and removal of soft solid layers, *J. Food Eng.,* **127** (2014) 24–33.

Yeckel. A. and Middleman, S. (1987) Removal of a viscous film from a rigid plane surface by an impinging liquid jet, *Chem. Eng. Comm*., **50**, 165-176.

Nomenclature

Roman

a	radial location of cleaning front	m
a_0	radius when cleaning front is first seen	m
a_x	radial location of cleaning front on jet path	m
a_{max}	radial location of cleaning front, limiting value	m
c	lumped parameter, Equation [5]	$kg^2\ m^{-4}\ s^{-1}$
d_N	nozzle throat diameter	m
k'	cleaning rate constant	$m\ s\ kg^{-1}$
K	lumped cleaning rate parameter, Equation [5]	$m\ s^{-0.2}$
M	momentum flux per unit width	$kg\ s^{-2}$
M_y	momentum flux per unit width to overcome yield stress	$kg\ s^{-2}$
$\dot{m}$	mass flow rate in jet	$kg\ s^{-1}$
p	radial distance to cleaning front, Equation [7]	m
Q	volumetric flow rate	$m^3\ s^{-1}$
R^2	correlation coefficient	-
r	radial co-ordinate	m
r_o	jet radius	m
R	radius of hydraulic jump	m
Re_{jet}	jet Reynolds number, defined $Re_{jet} = \rho U_o d_N/\mu$	-
S	swelling ratio, $S = \delta(t)/\delta_{dry}$	-
t	time	s
Δt	total time after cleaning front is first seen, $= t - t_0$	s
t_c	contact time of soil and water before jet breakthrough and	s

	cleaning starts	
t_o	time at which cleaning front, radius a_o, is first seen	s
U	mean velocity in film	m s^{-1}
U_o	jet and initial film mean velocity	m s^{-1}
v_{jet}	nozzle traverse speed (plate velocity with stationary jet)	m s^{-1}
w_c	width of cleaned region	m

Greek

β	contact angle	^{o}
δ	thickness of layer	m
δ_{dry}	thickness of dry layer, measured by micrometer	m
γ	surface tension (liquid/vapour)	N m^{-1}
μ	dynamic viscosity	Pa s
θ	azimuthal angle	^{o}
χ	slope of yield plane	^{o}
ρ	density	kg m^{-3}
τ_y	shear yield stress	Pa

Acronyms

CIP	cleaning in place
FDG	fluid dynamic gauging
PVA	polyvinylacohol
RFZ	radial flow zone
RO	reverse osmosis

Figure captions

Figure 1 Schematics showing (*a*) flow pattern created by horizontal jet impinging on vertical wall at impingement point O; (*b*) cleaning model, static jet (*c*) cleaning model, moving jet.

Figure 2 Proposed model for cleaning of a viscoplastic soil layer of thickness δ.

Figure 3 Schematic of moving jet apparatus

Figure 4 Slider blade device for creating soil layers. (*a*) schematic, side view; (*b*) photograph of coating PVA layer on Perspex.

Figure 5 Effect of nozzle-substrate motion on the film jump. Clean Perspex plate, d_N = 2 mm, Q = 35 mL s^{-1}. (*a*) Dimension R, measured at level of impingement. The v_{jet} error bars show the standard error in measurements of the steady plate velocity; (*b*) Photographs of impingement region for plate moving (*i*) downwards and (*ii*) upwards, v_{jet} = 52 mm s^{-1}.

Figure 6 Effect of initial PVA layer thickness δ_{dry} on initial contact time (left hand axis) before jet breakthrough was observed, and rupture time measured by FDG tests (Figure 7, right hand axis). 'Fingering', see Figure 8, was sometimes observed. Dashed locus shows linear relationship between t_c and δ for $\delta > 75$ µm. The error bars for δ_{dry} indicate the range in the thickness values measured across the plate.

Figure 7 Swelling ratio, $S = \delta(t)/\delta_{dry}$, describing swelling behaviour of PVA layers measured in RO water at 20°C by fluid dynamic gauging. Points marked R indicate where the layer was disrupted by the gauging flow: subsequent data were discarded. The small steps in each profile are related to changes in FDG nozzle position. The precision of the FDG measurements is ±10 µm and the steps lie within this range.

Figure 8 Photographs showing different removal patterns observed with PVA layers. (*a*) fingers, (*b*) annulus of uncleaned material, both for δ_{dry} = 105 ±20 µm; (*c*) evolution of initially asymmetric cleared region to a circular one; δ_{dry} = 43 ±22 µm.

Figure 9 Growth of cleared region for two different PVA layer thicknesses. Data are plotted in the form suggested by Equation [6] so that the gradient gives the value of K. Symbols – experimental measurements; loci – fitted trend lines. R^2 is the regression coefficient.

Figure 10 Effect of dry PVA layer thickness on K. Dashed locus shows mean value of K.

Figure 11 Cleaning of petroleum jelly layers with (*a*) static nozzle and (*b*) plate moving downwards; nozzle static. Perspex sheets. Experimental conditions: d_N = 2 mm, Q = 35 mL s^{-1}; (*a*) δ = 375 mm; (*b*) δ = 645 mm, v_{jet} = 7.3 mm s^{-1}.

Figure 12 Evolution of size of cleared region for petroleum jelly layers with static jet, d_N = 2 mm, Q = 35 mL s^{-1}. Symbols: circles, diamonds, this work, Perspex substrate, δ = 470 ± 50 µm; triangles, glass substrate, δ = 200 ± 30 µm, reported by Wang (2014). Solid loci show fit of initial data (solid symbols) to Equation [6]; dashed loci show fit for all data in a series to Equation [17]. Horizontal dot-dashed loci show a_{max}.

Figure 13 Effect of petroleum jelly layer thickness on cleaning model parameters. (*a*) *K* values, extracted from initial stages of cleaning (see Figure 12). Open circle, open triangle – mean values of *K* reported by Wilson *et al*. (2014) and Wang (2014), respectively, for a different petroleum jelly. PVA values (Figure 10) included for comparison. (*b*) Relationship between χ and *K*, calculated from a_{max} using Equation [10] and measured values of $\dot{m}$, δ and *c*: solid circles – this work, Perspex substrate, τ_y = 50 Pa; triangle, Wang (2014), glass substrate (see Figure 12), τ_y = 12 Pa

Figure 14 Shape of petroleum jelly cleaning front for v_{jet} = 8 mm s^{-1} for layers of thickness (*a*) 850 μm and (*b*) 590 μm with a fixed jet and (*i*) substrate moving upwards and (*ii*) substrate moving downwards. Data are normalised by distance a_x (see Figure 1(*c*)) which was extracted directly from photographs. Loci show predictions of moving jet model (Equation [7]).

Figure 15 Effect of nozzle-substrate velocity on width of cleaned region for two values of petroleum jelly layer thickness. Data are presented in the form suggested by Equation [8]: loci show lines of best fit, the gradients of which are used to determine *K*.

Figure 16 Effect of petroleum jelly layer thickness on *K* obtained from moving jet experiments. Static nozzle results (Figure 13(*a*)) plotted for comparison.

Supplementary Materials

Supplementary Figure S1: Effect of jet flow rate on RFZ radius with jet flow rate for different nozzle diameters (*a*) d_N = 2 mm, (*b*) d_N = 3 mm, (*c*) d_N = 4 mm on (*i*) Perspex and (*ii*) glass. *x*-axis error bars are too small to plot. Eq. [3] is plotted using the measured advancing contact angles (solid) and an effective contact angle of 90° (dashed).

Supplementary Video 1 Cleaning of PVA layer (δ = 93 µm) on Perspex, static nozzle (d_N = 2 mm, $\dot{m}$ = 35 g s^{-1})

Supplementary Video 2 Cleaning of petroleum jelly layer (δ = 136 µm) on Perspex, static nozzle (d_N = 2 mm, $\dot{m}$ = 35 g s^{-1})

Supplementary Video 3 Cleaning of petroleum jelly layer (δ = 645 µm) on Perspex, moving nozzle (d_N = 2 mm, = 7.3 mm s^{-1}, $\dot{m}$ = 35 g s^{-1})

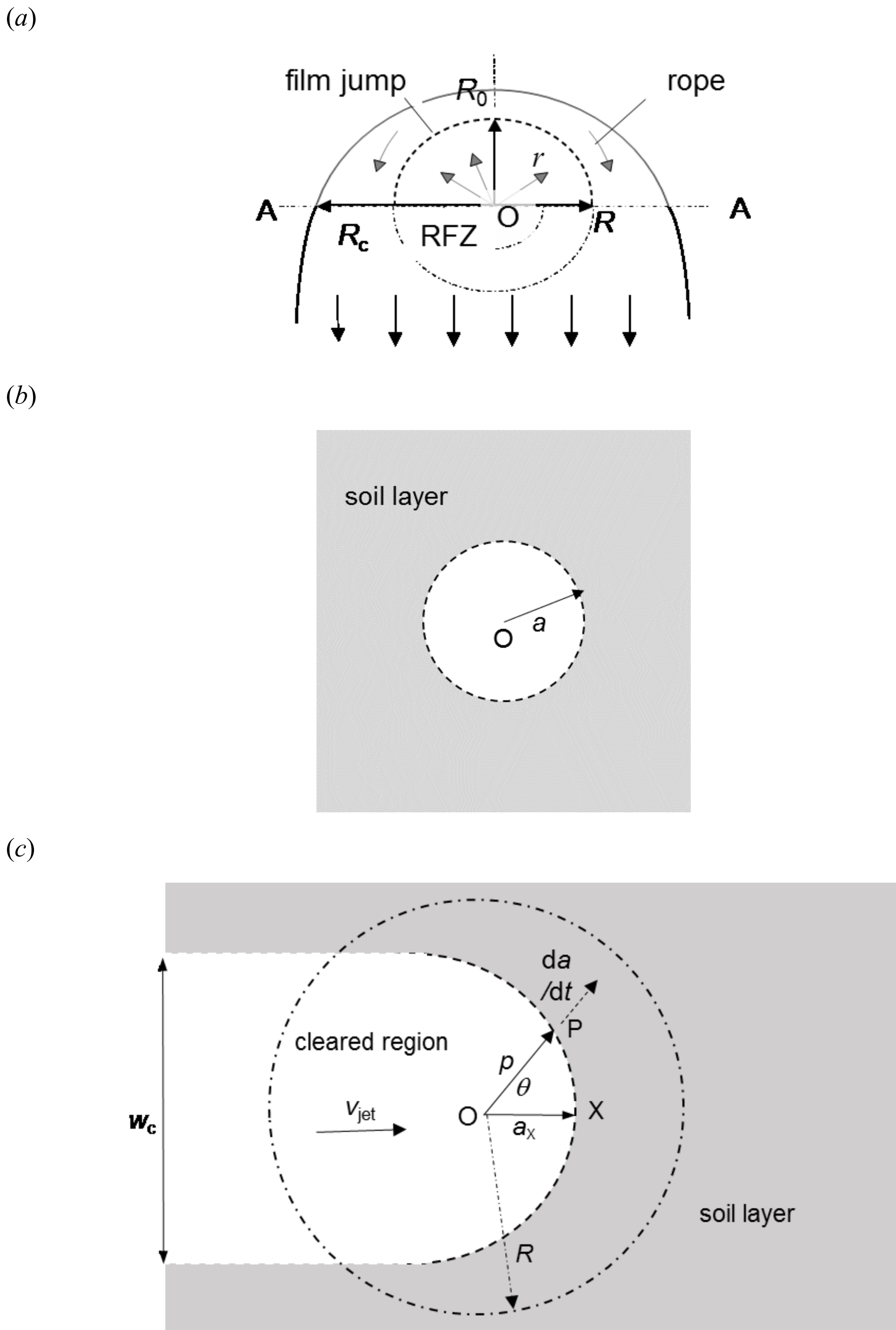

Figure 1 Schematics showing (*a*) flow pattern created by horizontal jet impinging on vertical wall at impingement point O; (*b*) cleaning model, static jet (*c*) cleaning model, moving jet.

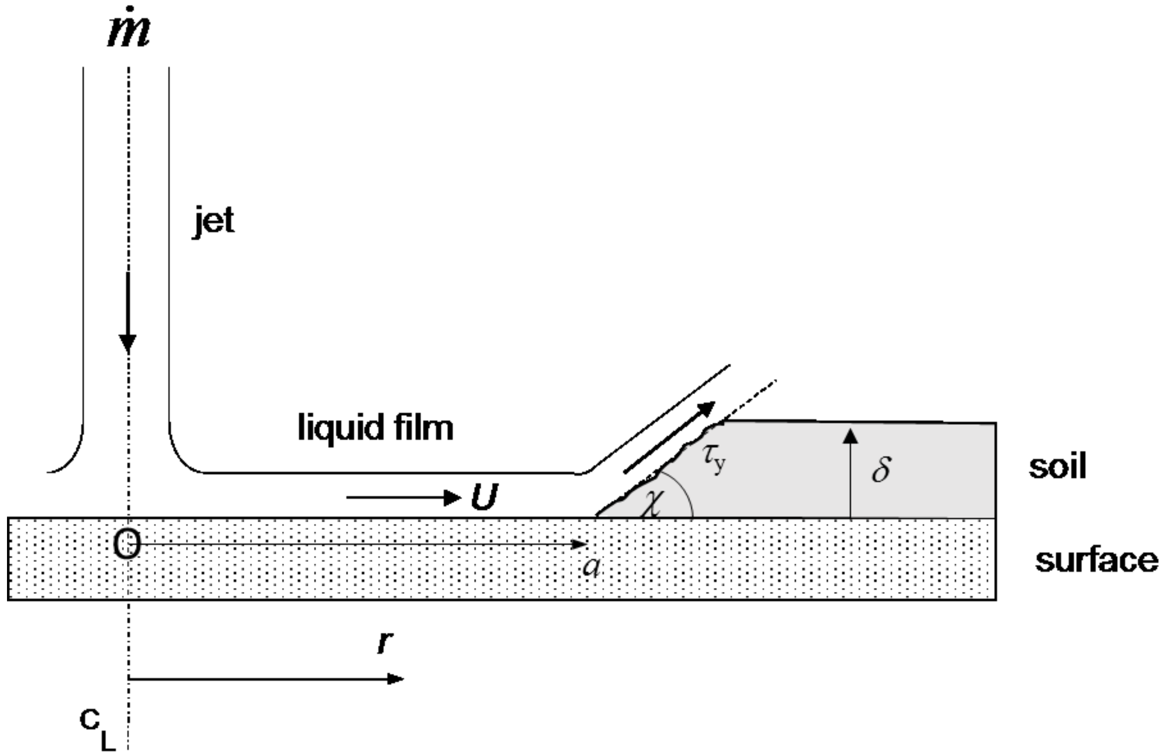

Figure 2 Proposed model for cleaning of a viscoplastic soil layer of thickness δ.

Figure 3 Schematic of moving jet apparatus

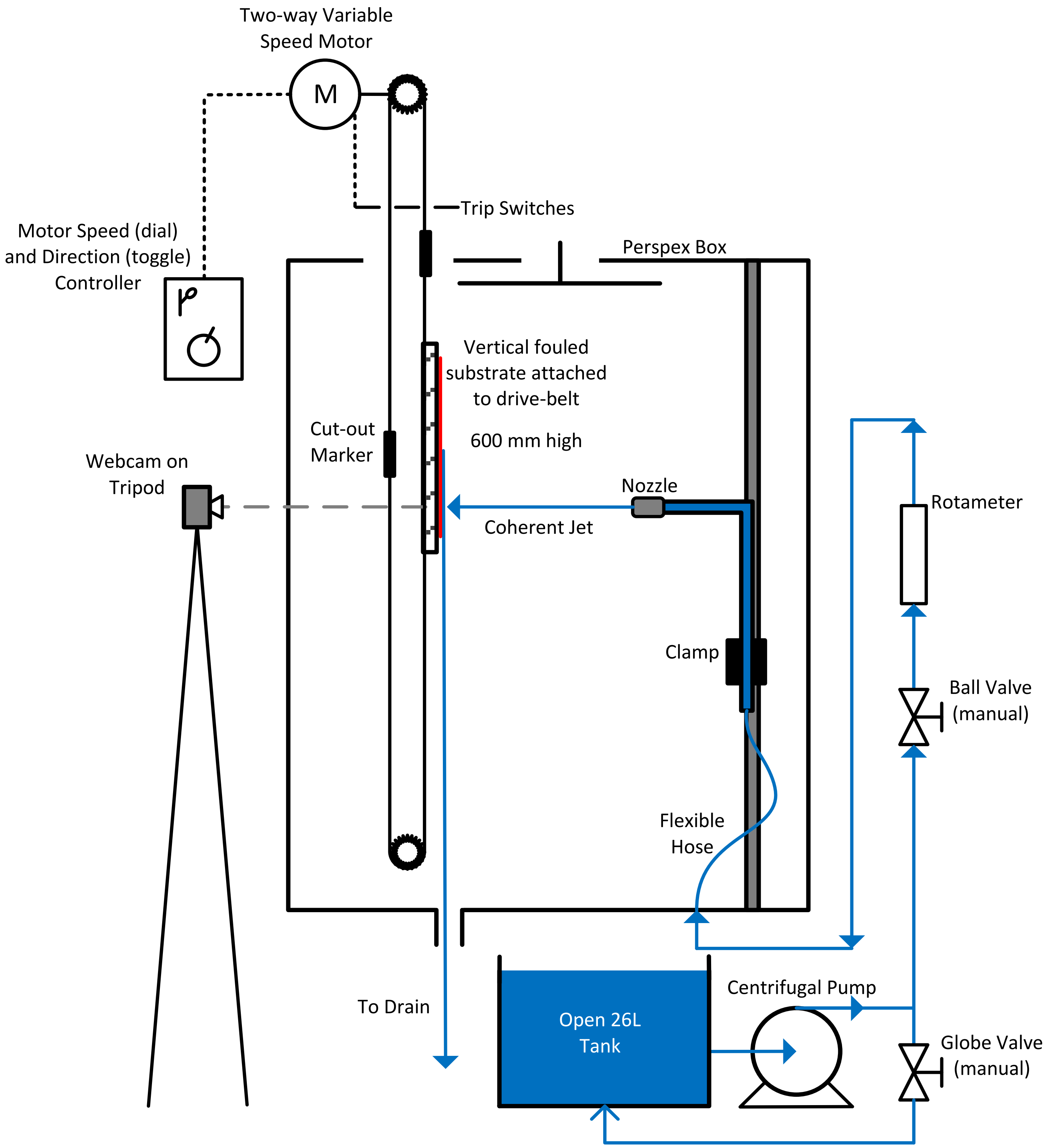

(*a*)

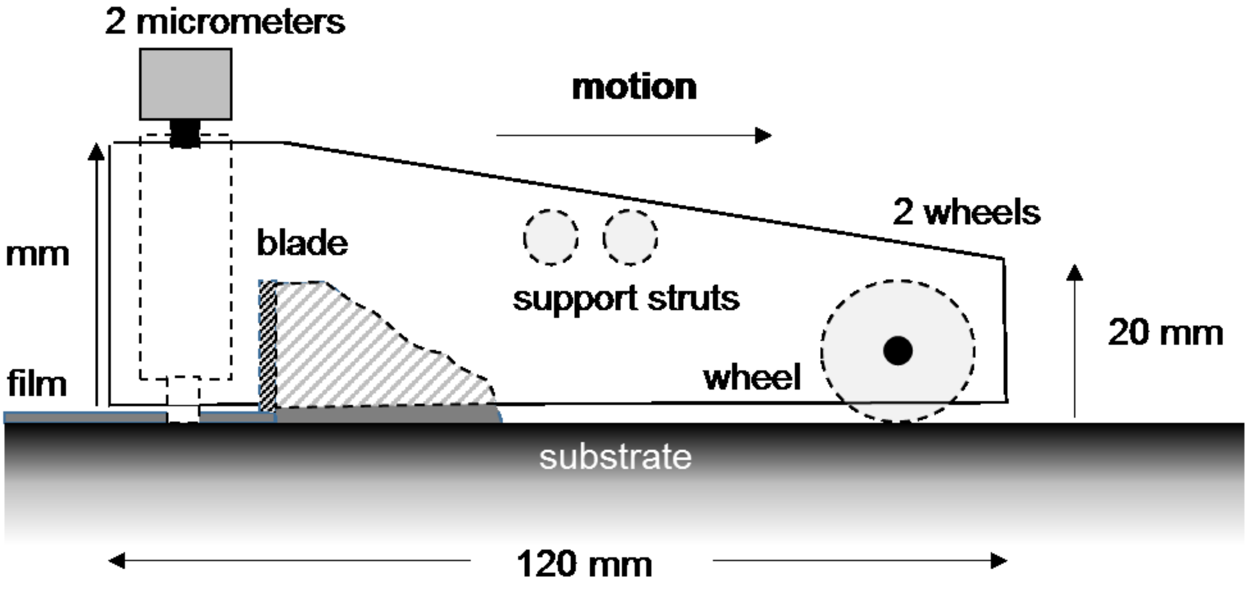

(*b*)

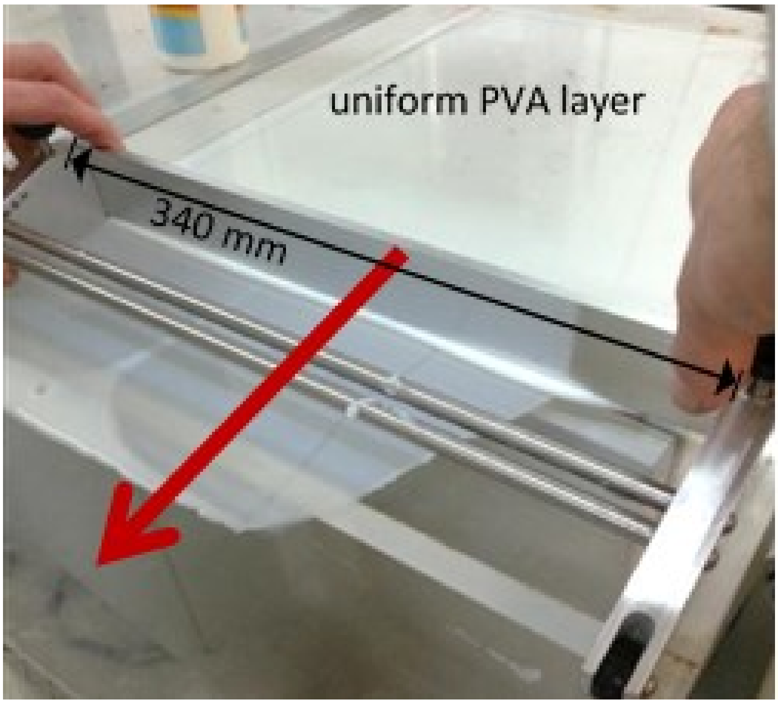

Figure 4 Slider blade device for creating soil layers. (*a*) schematic, side view; (*b*) photograph of coating PVA layer on Perspex.

(*a*)

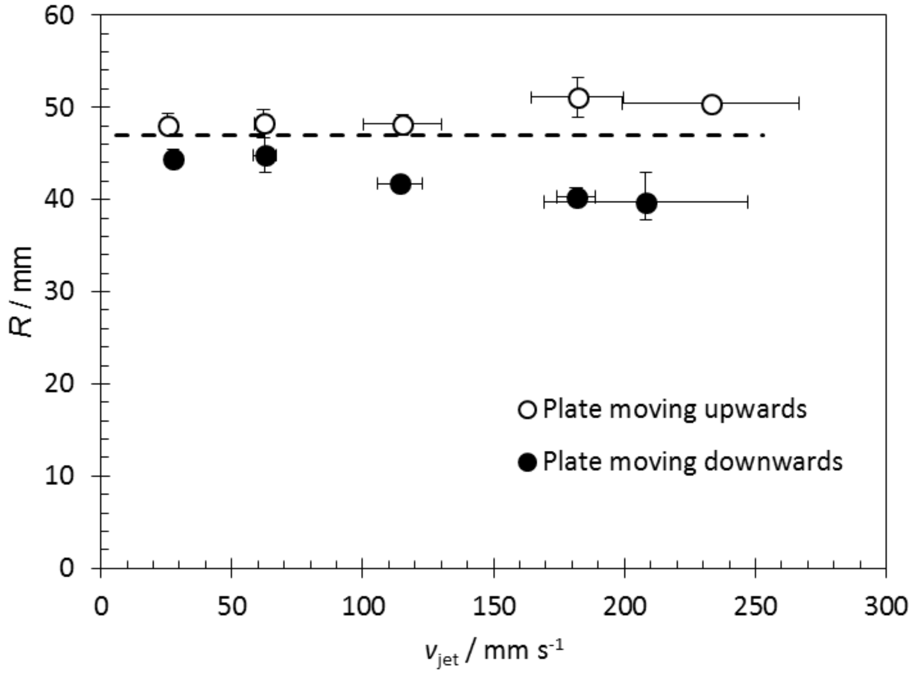

(*b*) (*i*) (*ii*)

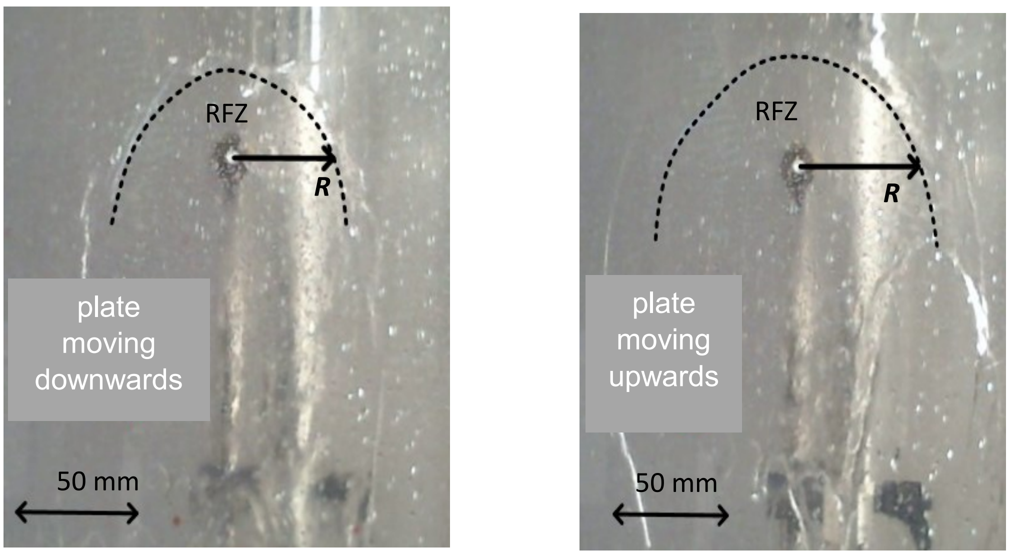

Figure 5 Effect of nozzle-substrate motion on the film jump. Clean Perspex plate, d_N = 2 mm, Q = 35 mL s^{-1}. (*a*) Dimension *R*, measured at level of impingement. The v_{jet} error bars show the standard error in measurements of the steady plate velocity; (*b*) Photographs of impingement region for plate moving (*i*) downwards and (*ii*) upwards, v_{jet} = 52 mm s^{-1}.

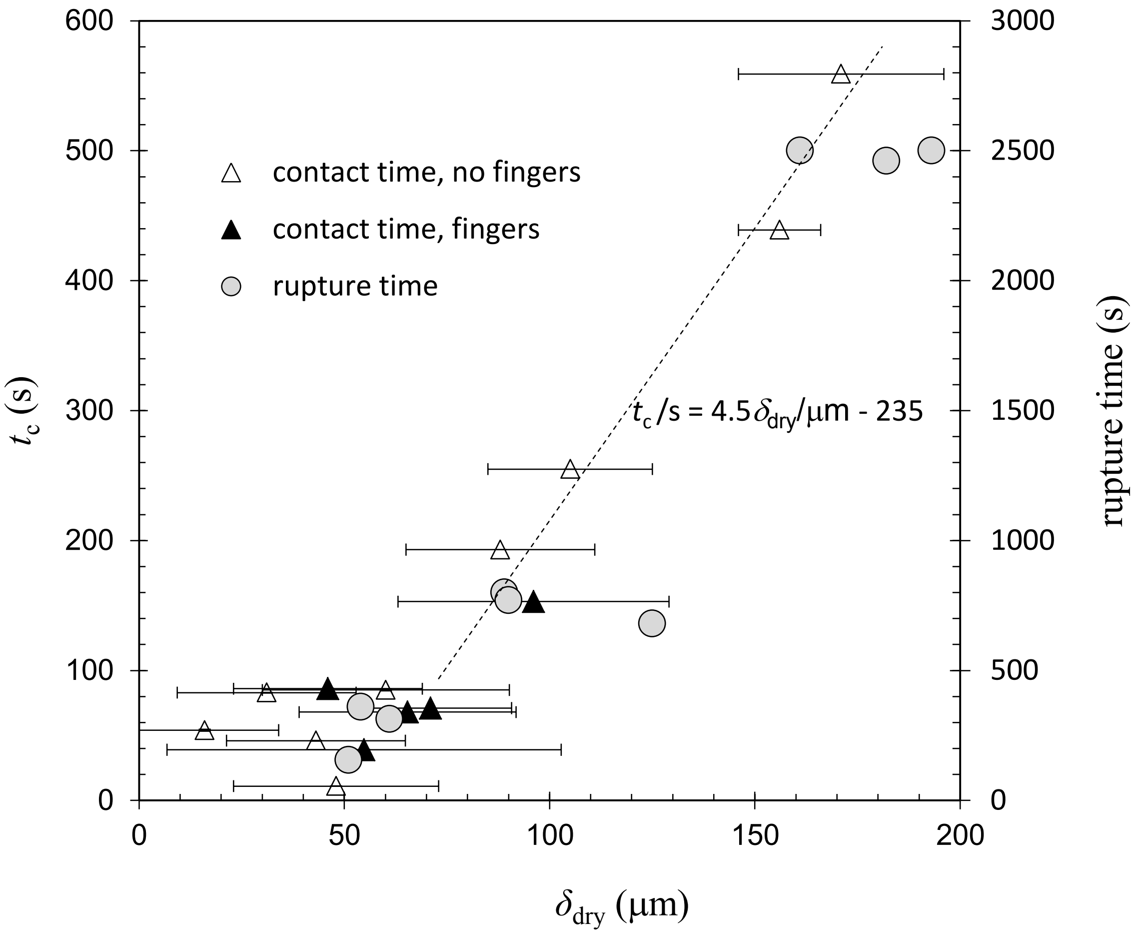

Figure 6 Effect of initial PVA layer thickness δ_{dry} on initial contact time (left hand axis) before jet breakthrough was observed, and rupture time measured by FDG tests (Figure 7, right hand axis). 'Fingering', see Figure 8, was sometimes observed. Dashed locus shows linear relationship between t_c and δ for $\delta > 75$ µm. The error bars for δ_{dry} indicate the range in the thickness values measured across the plate.

.

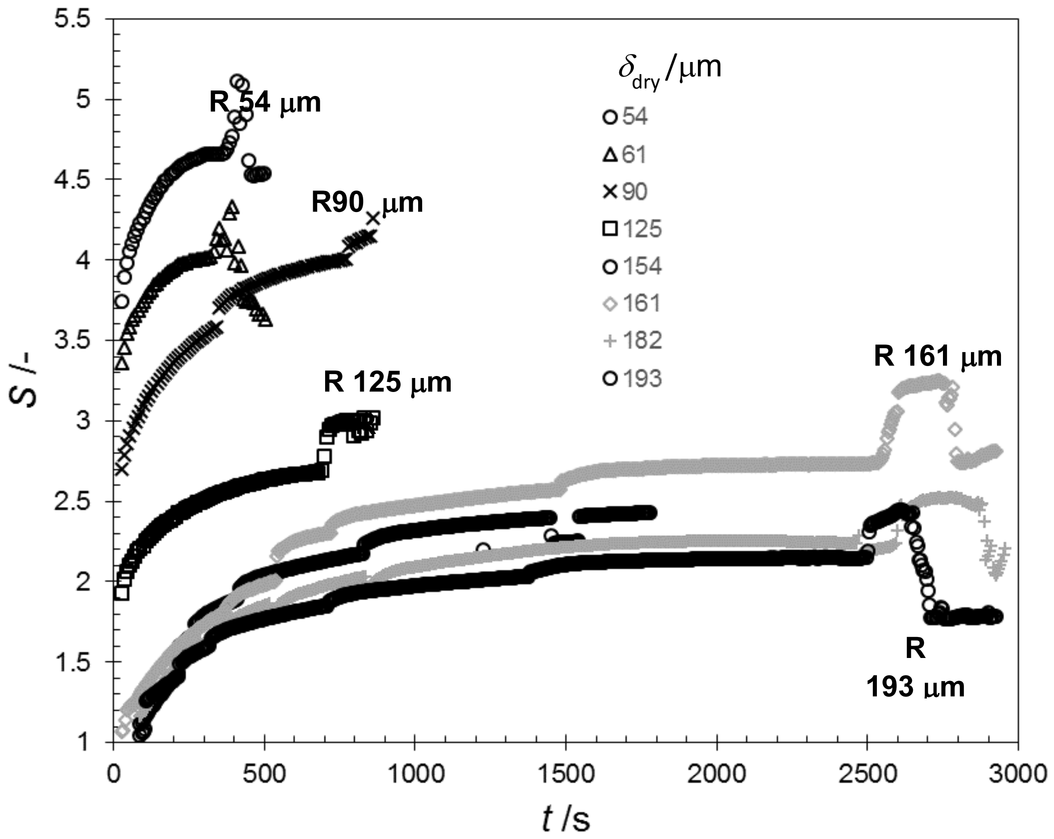

Figure 7 Swelling ratio, $S = \delta(t)/\delta_{dry}$, describing swelling behaviour of PVA layers measured in RO water at 20°C by fluid dynamic gauging. Points marked R indicate where the layer was disrupted by the gauging flow: subsequent data were discarded. The small steps in each profile are related to changes in FDG nozzle position. The precision of the FDG measurements is ±10 μm and the steps lie within this range.

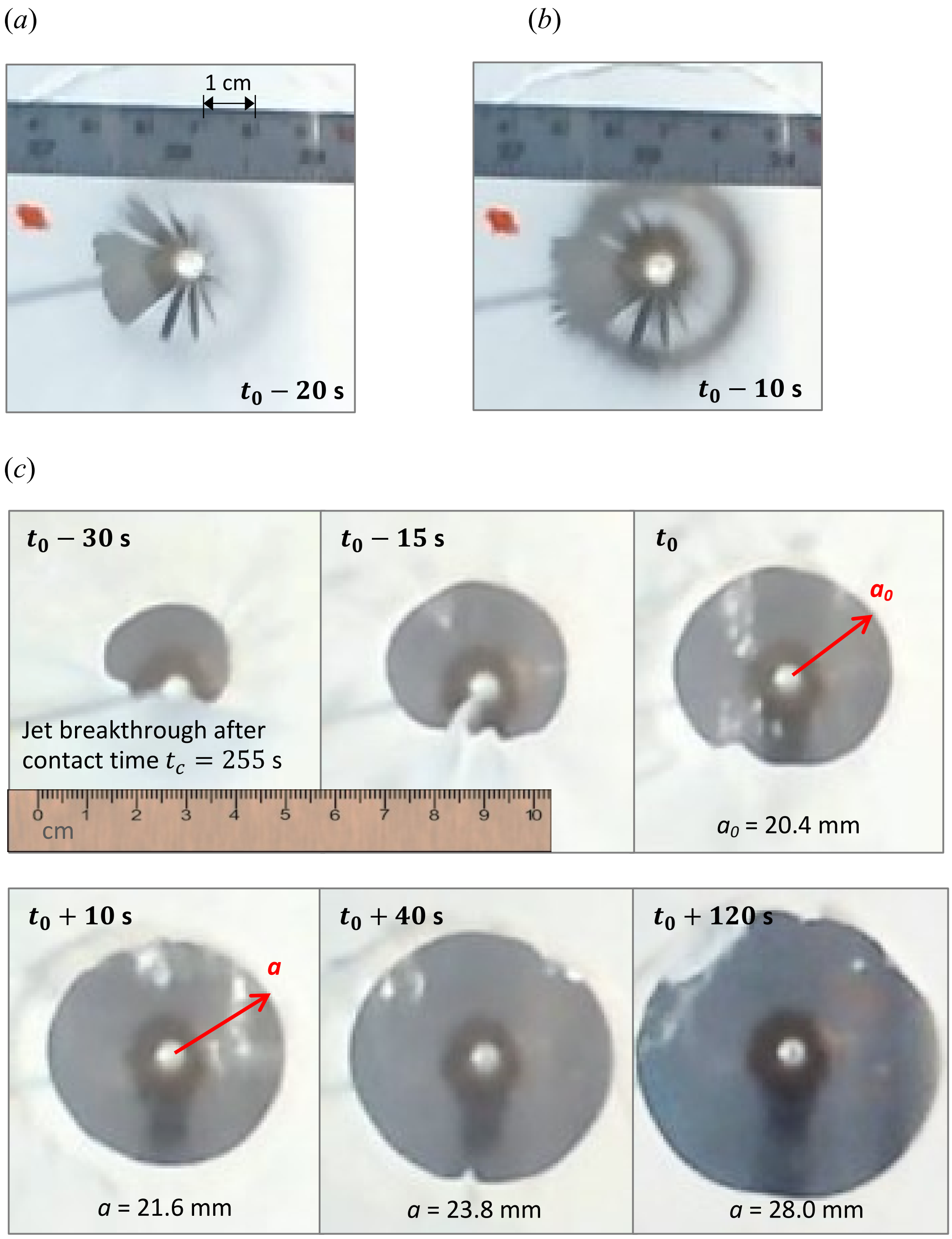

Figure 8 Photographs showing different removal patterns observed with PVA layers. (*a*) fingers, (*b*) annulus of uncleaned material, both for δ_{dry} = 105 ±20 μm; (*c*) evolution of initially asymmetric cleared region to a circular one; δ_{dry} = 43 ±22 μm.

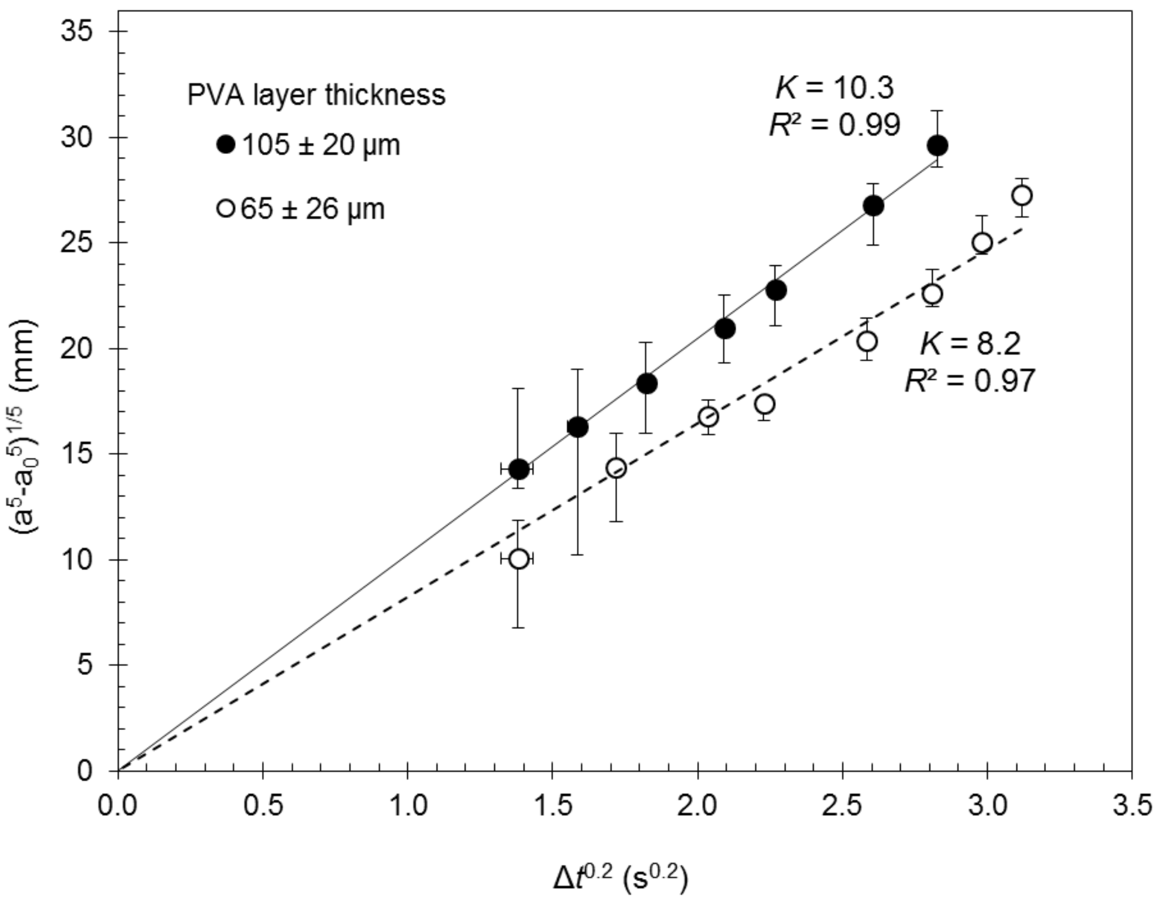

Figure 9 Growth of cleared region for two different PVA layer thicknesses. Data are plotted in the form suggested by Equation [6] so that the gradient gives the value of *K*. Symbols – experimental measurements; loci – fitted trend lines. R^2 is the regression coefficient.

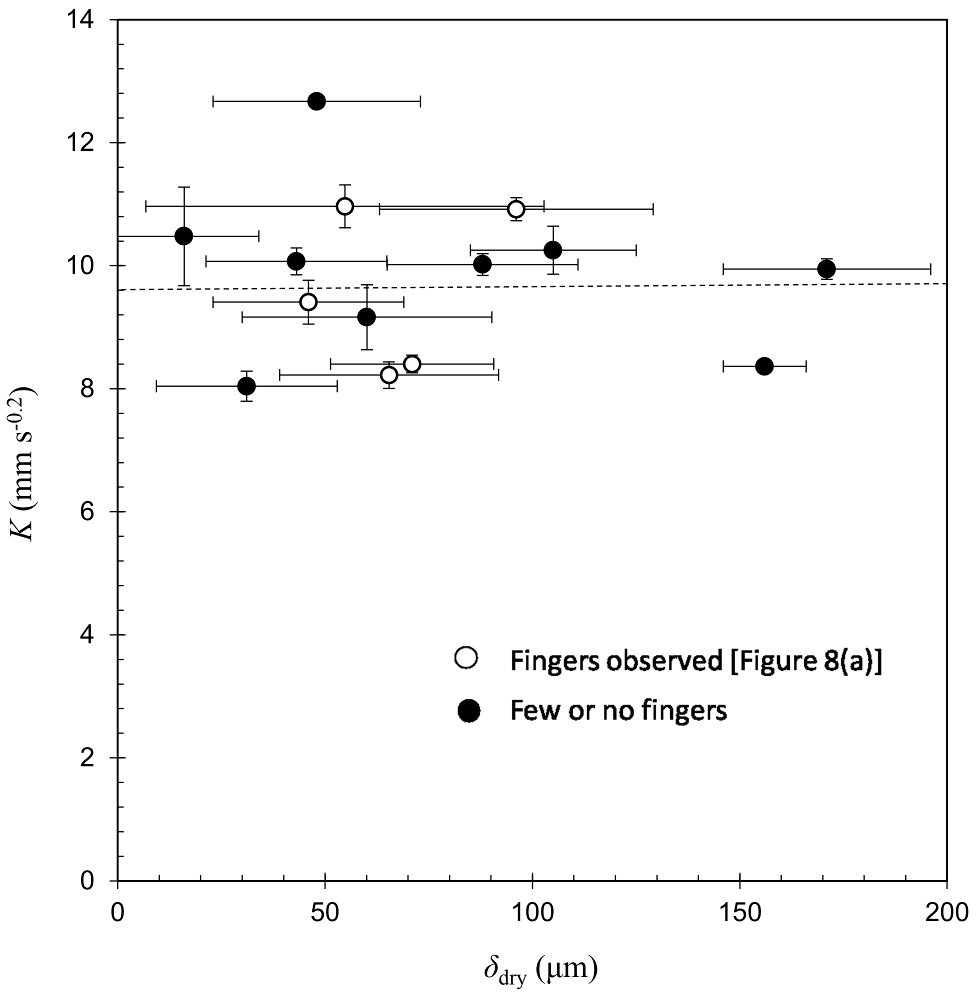

Figure 10 Effect of dry PVA layer thickness on K. Dashed locus shows mean value of K.

(*a*)

(*b*)

Figure 11 Cleaning of petroleum jelly layers with (*a*) static nozzle and (*b*) plate moving downwards; nozzle static. Perspex sheets. Experimental conditions: d_N = 2 mm, Q = 35 mL s^{-1}; (*a*) δ = 375 mm; (*b*) δ = 645 mm, v_{jet} = 7.3 mm s^{-1}.

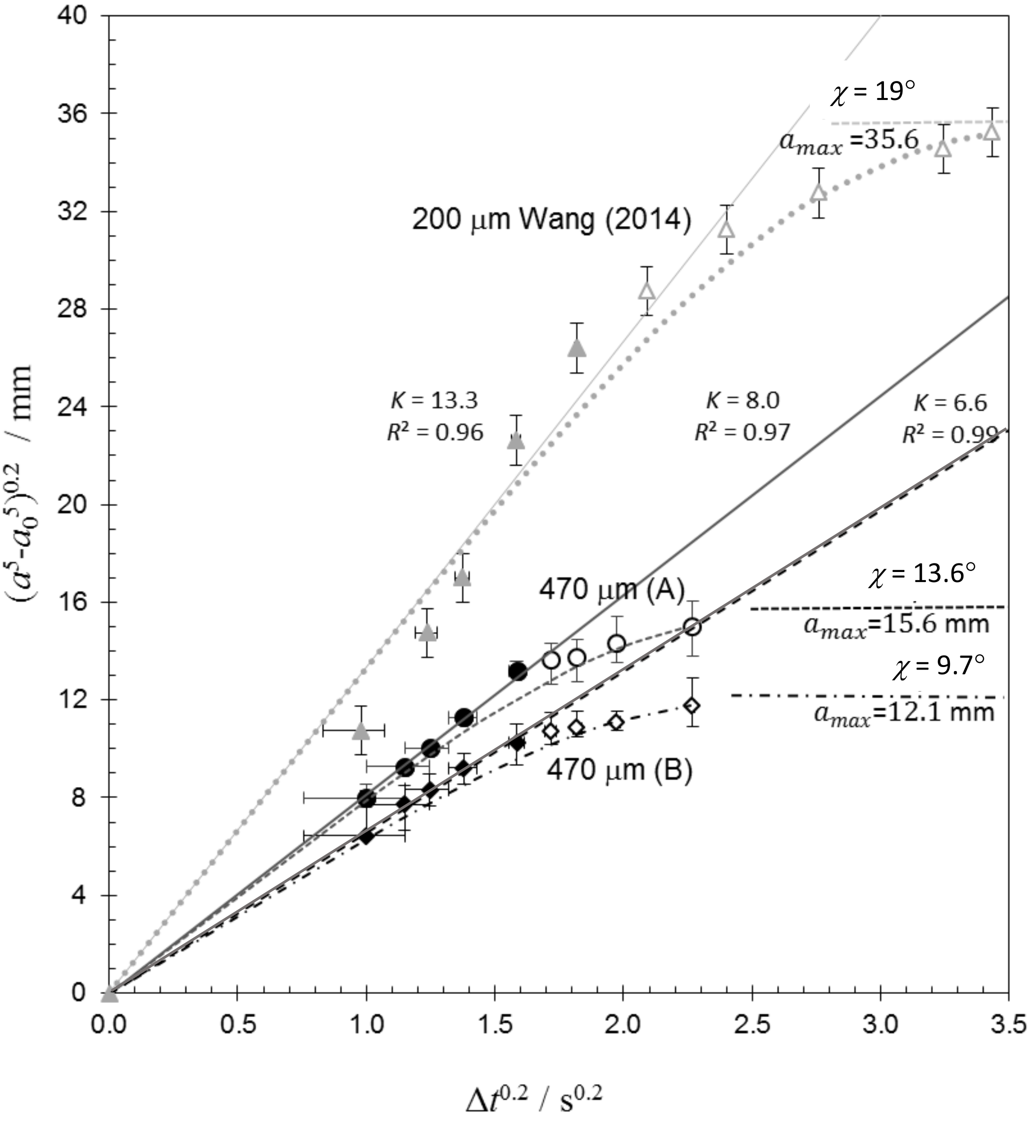

Figure 12 Evolution of size of cleared region for petroleum jelly layers with static jet, d_N = 2 mm, Q = 35 mL s^{-1}. Symbols: circles, diamonds, this work, Perspex substrate, δ = 470 ± 50 μm; triangles, glass substrate (different petroleum jelly), δ = 200 ± 30 μm, reported by Wang (2014). Solid loci show fit of initial data (solid symbols) to Equation [6]; dashed loci show fit for all data in a series to Equation [17]. Horizontal loci show a_{max}.

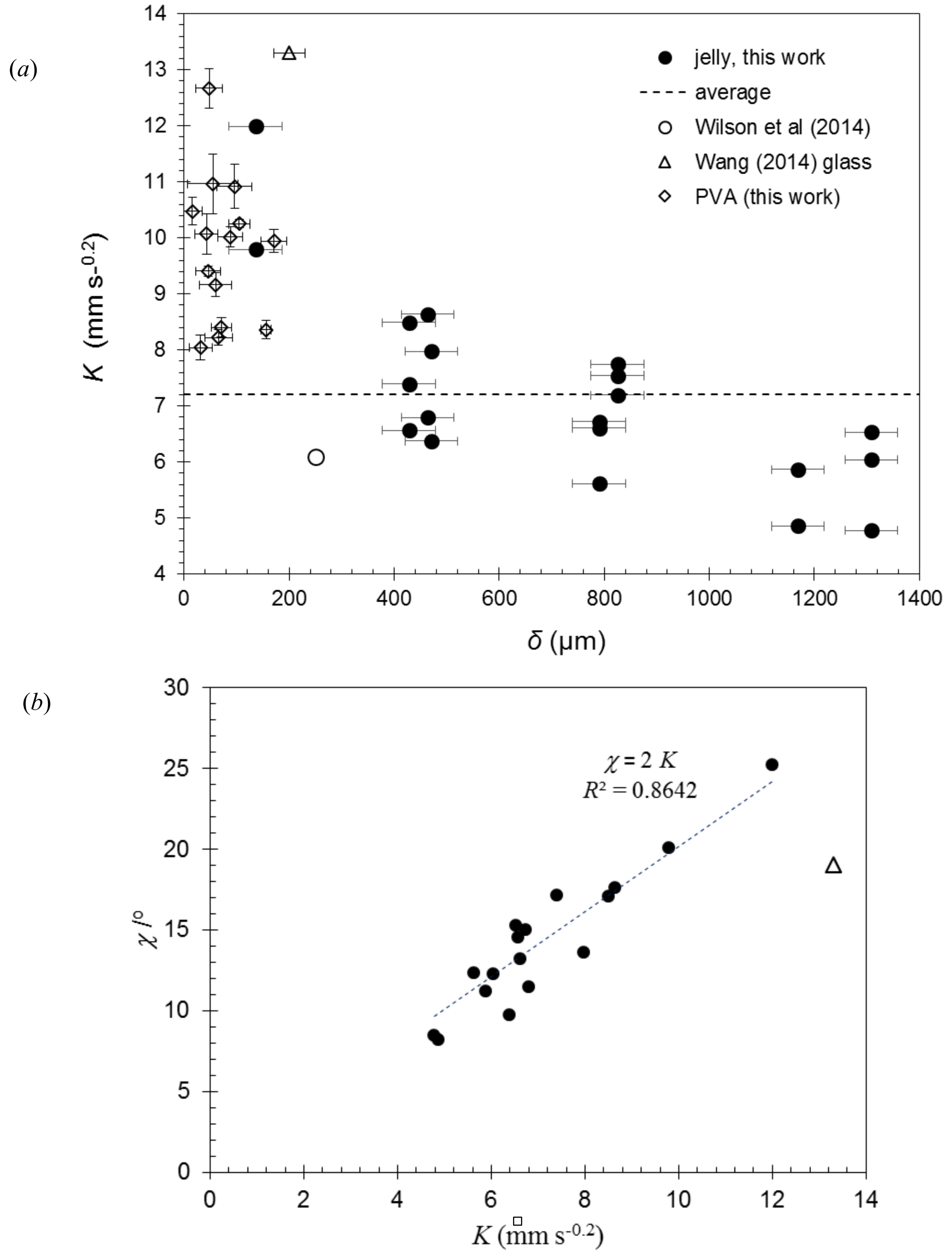

Figure 13 Effect of petroleum jelly layer thickness on cleaning model parameters. (*a*) *K* values, extracted from initial stages of cleaning (see Figure 12). Open circle, open triangle – mean values of *K* reported by Wilson *et al*. (2014) and Wang (2014), respectively, for a different petroleum jelly. PVA values (Figure 10) included for comparison. (*b*) Relationship between χ and *K*, calculated from a_{max} using Equation [10] and measured values of $\dot{m}$, δ and *c*: solid circles – this work, Perspex substrate, τ_y = 50 Pa; triangle, Wang (2014), glass substrate (see Figure 12), τ_y = 12 Pa.

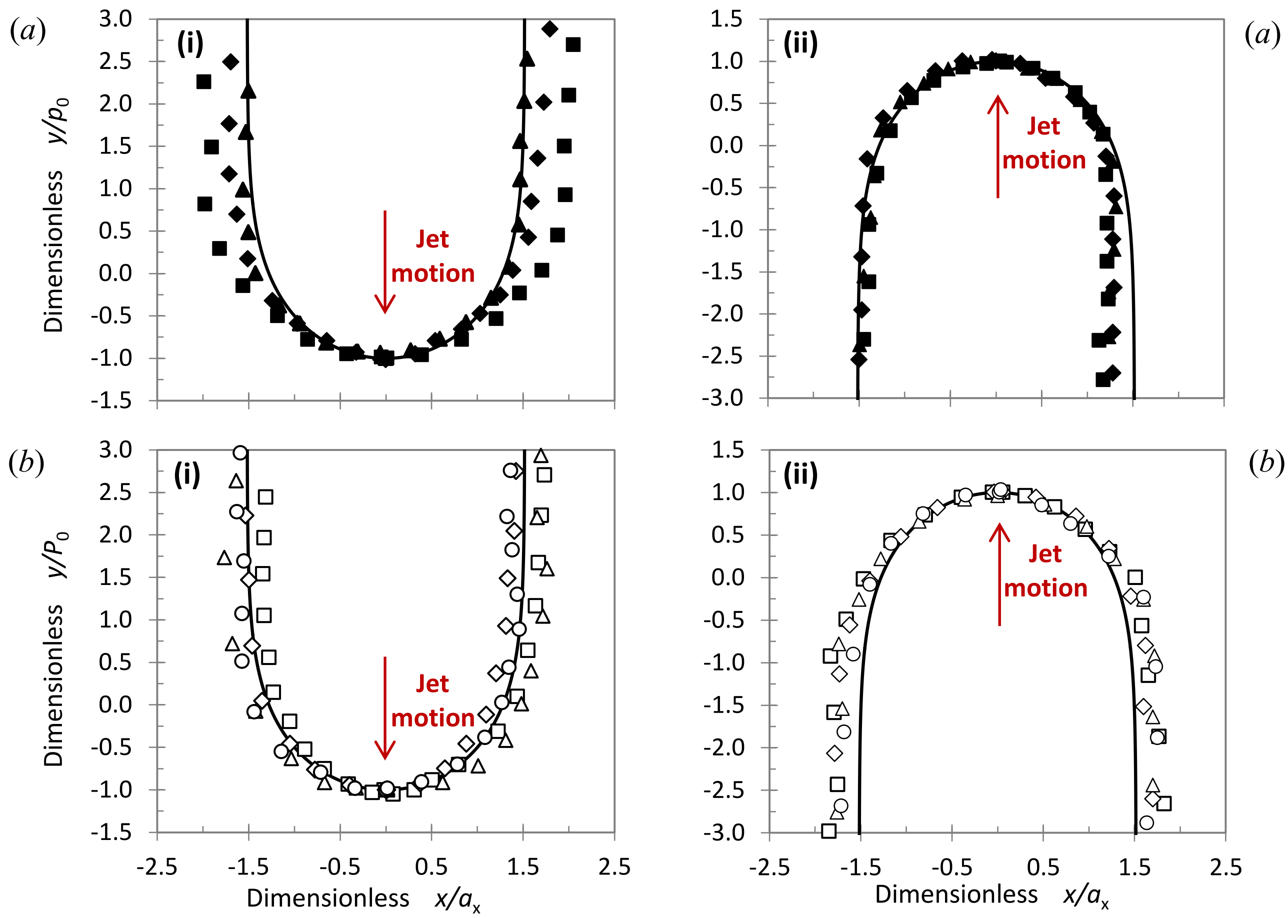

Figure 14 Shape of petroleum jelly cleaning front for v_{jet} = 8 mm s^{-1} for layers of thickness (*a*) 850 μm and (*b*) 590 μm with a fixed jet and (*i*) substrate moving upwards and (*ii*) substrate moving downwards. Data are normalised by distance a_x (see Figure 1(*c*)) which was extracted directly from photographs. Loci show predictions of moving jet model (Equation [7]).

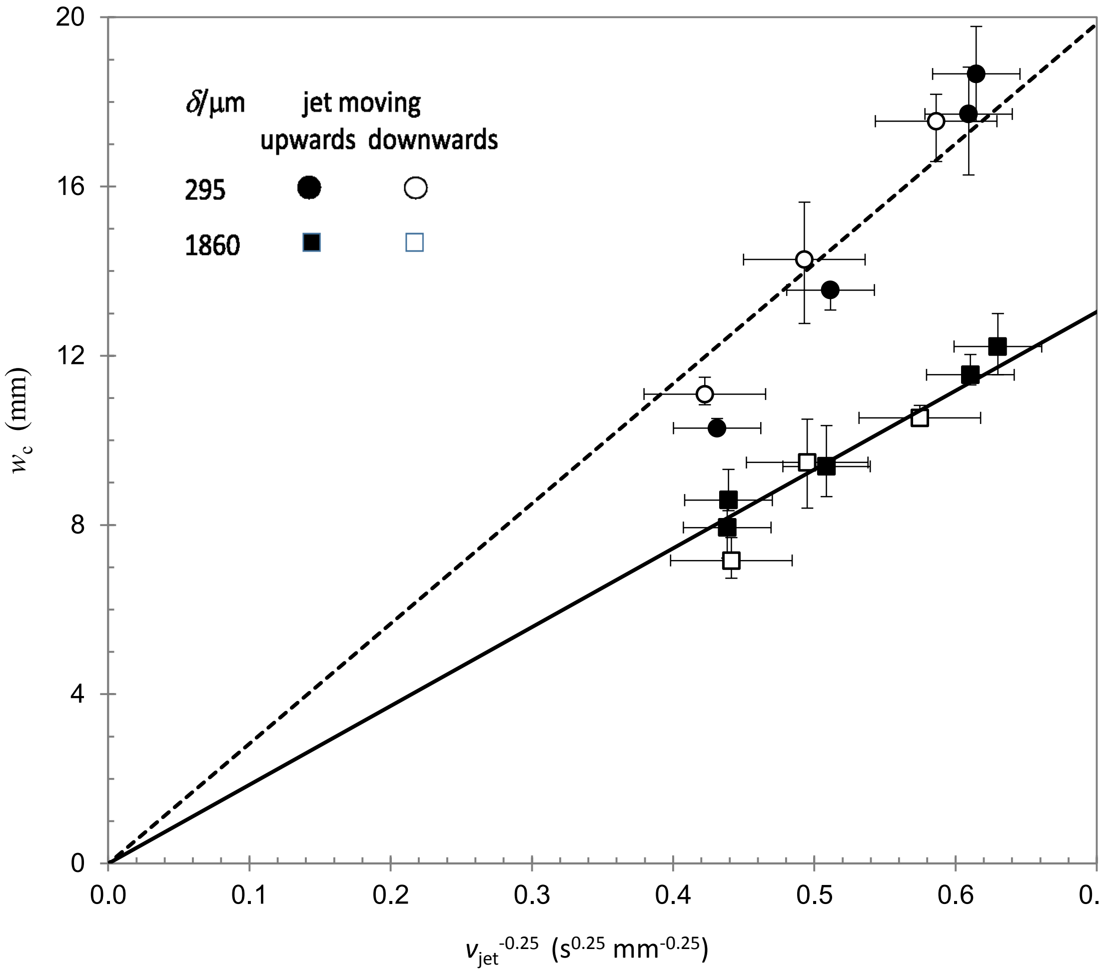

Figure 15 Effect of nozzle-substrate velocity on width of cleaned region for two values of petroleum jelly layer thickness. Data are presented in the form suggested by Equation [8]: loci show lines of best fit, the gradients of which are used to determine *K*.

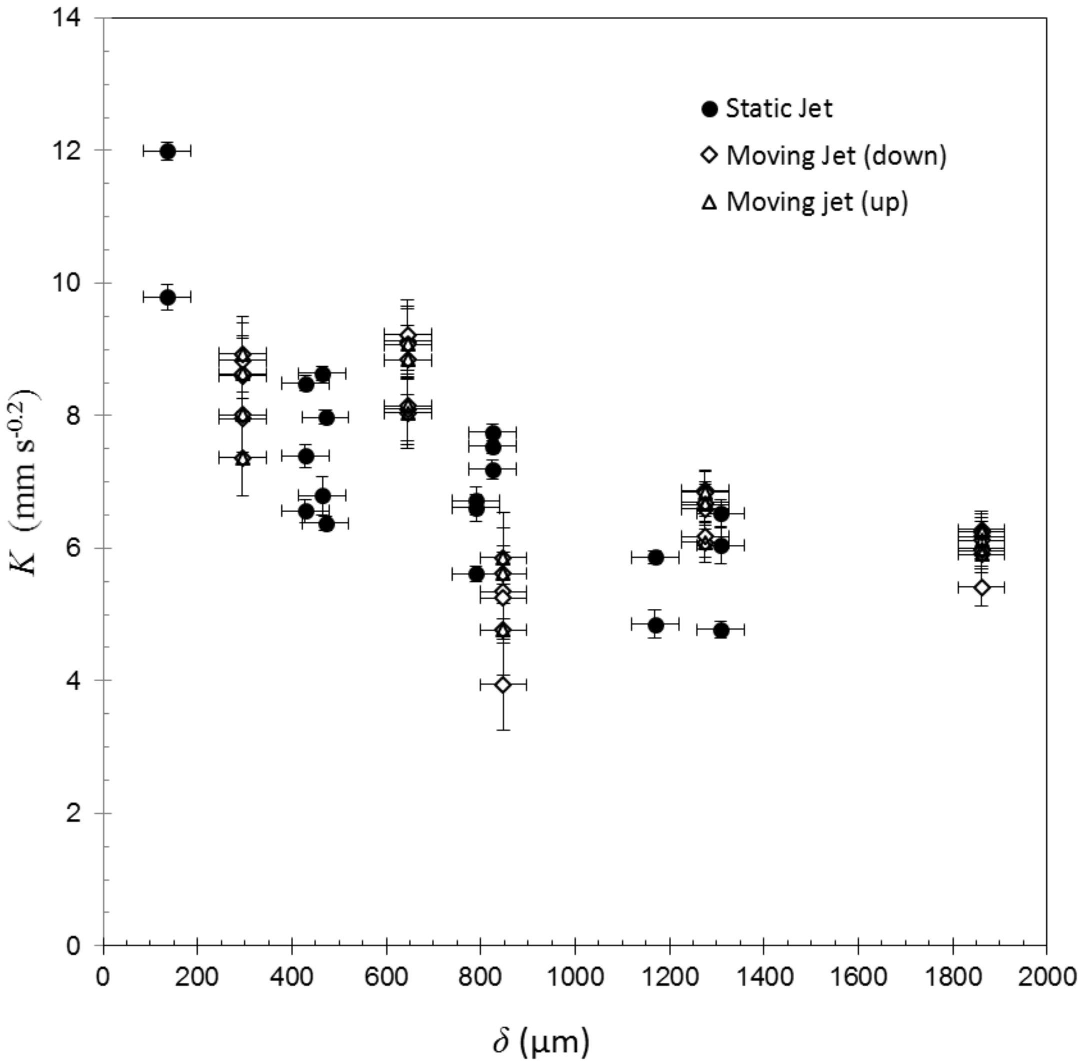

Figure 16 Effect of petroleum jelly layer thickness on K obtained from moving jet experiments. Static nozzle results (Figure 13(a)) plotted for comparison.

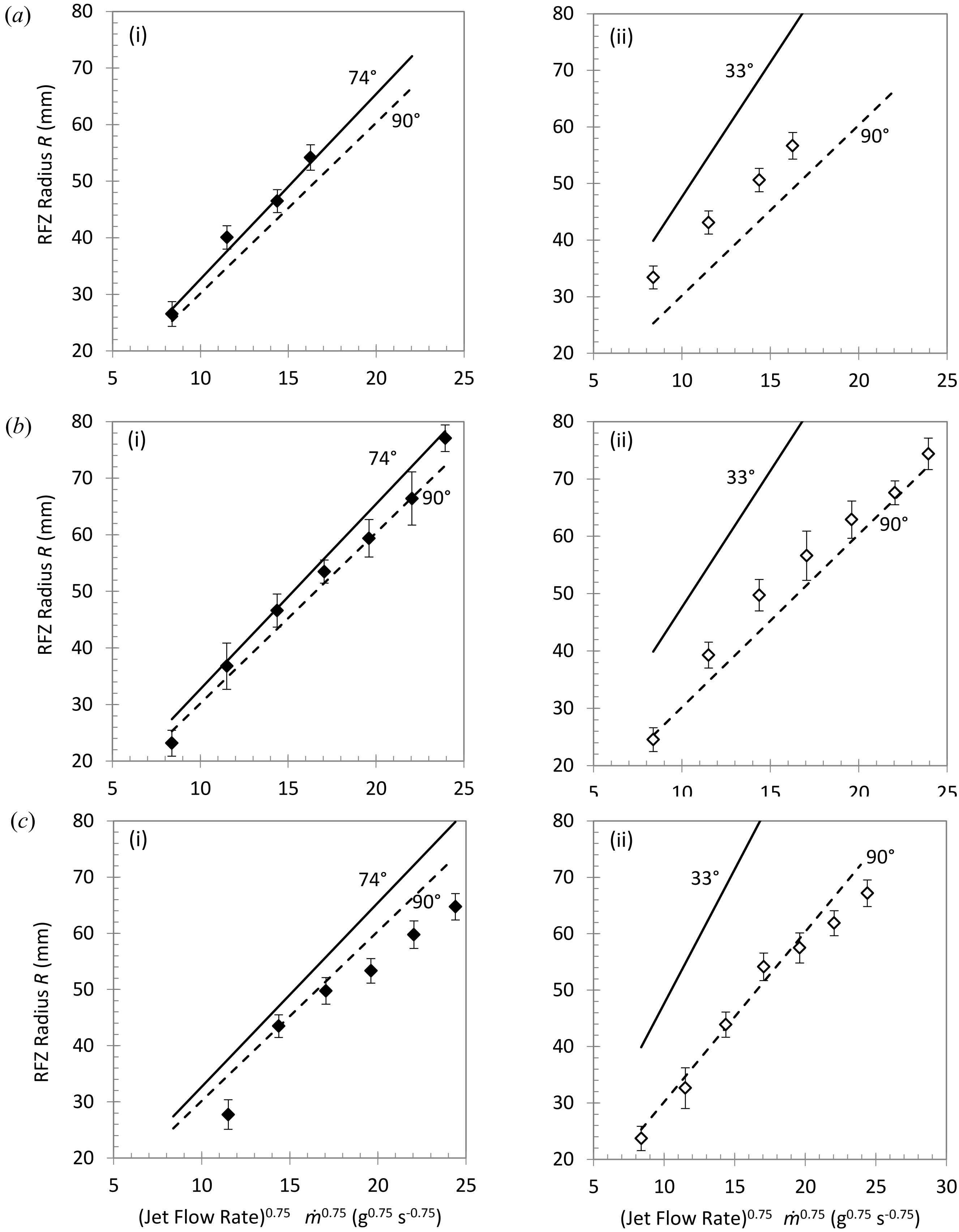

Supplementary Figure S1: Effect of jet flow rate on RFZ radius with jet flow rate for different nozzle diameters (*a*) d_N = 2 mm, (*b*) d_N = 3 mm, (*c*) d_N = 4 mm on (*i*) Perspex and (*ii*) glass. *x*-axis error bars are too small to plot. Eq. [3] is plotted using the measured advancing contact angles (solid) and an effective contact angle of 90° (dashed).